LAWRENCE
LIVERMORE
NATIONAL
LABORATORY

LLNL-TR-654049

California GAMA Special Study: Geostatistical analysis of groundwater age and other noble gas derived parameters in California groundwater

Ate Visser, Jean E. Moran*,
Michael J. Singleton, and Bradley K. Esser

Lawrence Livermore National Laboratory
**California State University, East Bay*

October 2014

Draft Report for the California State Water Resources Control Board

GAMA Special Studies Task 12.4: *Groundwater Age Database and Map*

Disclaimer

Auspices Statement

This work performed under the auspices of the U.S. Department of Energy by Lawrence Livermore National Laboratory under Contract DE-AC52-07NA27344.

GAMA: AMBIENT GROUNDWATER MONITORING & ASSESSMENT PROGRAM SPECIAL STUDY

California GAMA Special Study:
Geostatistical analysis of groundwater age and other noble gas derived parameters in California

Ate Visser, Jean E. Moran, Michael J. Singleton, and Bradley K. Esser*

Lawrence Livermore National Laboratory
**California State University, East Bay*

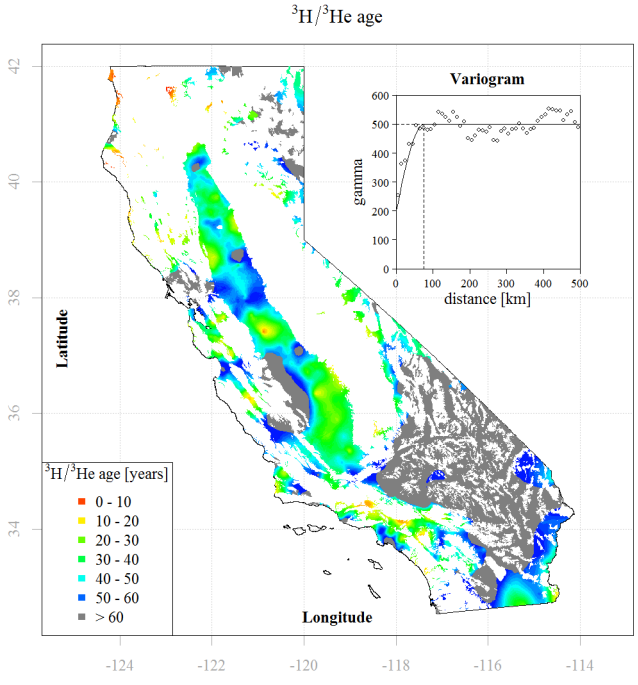

Prepared in cooperation with the
California State Water Resource Control Board
LLNL-TR- 654049

October 2014

Suggested citation:
Ate Visser, Jean E. Moran, Michael J. Singleton, and Bradley K. Esser (2014) California GAMA Special Study: **Geostatistical analysis of groundwater age and other noble gas derived parameters in California**. Lawrence Livermore National Laboratory LLNL-TR-654049, 44 pp.

California GAMA Special Study: Geostatistical analysis of groundwater age and other noble gas derived parameters in California

A. Visser, J. E. Moran*, M. J. Singleton, and B. K. Esser:
*Lawrence Livermore National Laboratory, *California State University-East Bay*
Prepared in cooperation with the State Water Resources Control Board

Key Points

- Noble gas, tritium and water stable isotope analyses on California groundwater samples collected for the GAMA program were assembled into a state-wide data set.
- The state-wide data set was subjected to geostatistical analysis to reveal patterns related to recharge, groundwater residence time, and large-scale groundwater management. Variables of interest were mapped by means of kriging prediction.
- Noble gas derived parameters (recharge temperature, excess air, terrigenic helium-4, terrigenic helium isotope ratio and tritiogenic helium-3) were calculated using the unfractionated excess air (UA) model with a recharge elevation assumed to be the well head elevation. The local terrigenic helium isotope ratio was derived from a geostatistical interpolation and subsequently used in separating the tritiogenic helium component in each sample.
- In total, 1630 $^{3}H/^{3}He$ ages are presented, in addition to 977 samples with less than 1 pCi/L (and assigned an age of 60 years).
- Young $^{3}H/^{3}He$ ages delineating areas of groundwater recharge are found along the major, perennial rivers in the Central Valley, in the forebay areas of major coastal basins dominated by managed aquifer recharge, along the northern California coast, and along the eastern slopes of the Sierra Nevada. In large portions of southeastern California, tritium-free, fossil groundwater predominates, while modern groundwater abstracted in this area is found only near distributaries of the Colorado River, which has recharged under distinctly different conditions.
- Tritium concentrations in the Central Valley are largely determined by the mixing of pre-modern (^{3}H free) groundwater with modern groundwater (containing ^{3}H) and not by decay of atmospheric tritium. In basins with managed aquifer recharge operations, tritium concentrations are more strongly determined by the initial tritium concentrations in specific historical recharge periods than by mixing of modern and pre-modern groundwater.
- Noble gas recharge temperatures range from 25 °C in the Mojave Desert to below 10 °C in the Sierra Nevada. Because of strong elevation gradients, local anomalies in groundwater recharge temperatures are difficult to distinguish on the map of noble gas recharge temperatures. However, managed aquifer recharge operations have a major impact on signatures of recharge, including patterns in stable isotopes and noble gas recharge temperatures.
- The depth to tritium-free groundwater typically varies between 100 and 400 ft. Several areas, including Santa Clara River Valley, San Gabriel Basin, portions of the Mojave Basin, the Los Angeles physiographic basin, and the area between Davis and Sacramento, stand out as having a very deep boundary between modern and pre-modern groundwater. On the other hand, tritium-free groundwater is found at shallow depths in the Volcanic Highlands of the North San Francisco Study Unit and in the Indian Wells area of the Basin and Range province.

Table of Contents

California GAMA Special Study: Geostatistical analysis of groundwater age and other noble gas derived parameters in California

A. Visser, J. E. Moran*, M. J. Singleton, and B. K. Esser:
*Lawrence Livermore National Laboratory, *California State University-East Bay*
Prepared in cooperation with the State Water Resources Control Board

1 INTRODUCTION

Water is a limited resource in California. While some areas receive over 3000 mm of precipitation per year, a large proportion of the population is located in areas receiving less than 500 mm per year. Most precipitation falls in winter and a large proportion of precipitation falls as snow in the Sierra Nevada mountain range. Snowmelt contribution to rivers draining the Sierra Nevada causes peak discharge to occur in late spring. Reservoirs mitigate flood risk and store snowmelt to be released gradually in summer. The groundwater system acts as a natural buffer for seasonal and inter-annual precipitation variability. Historically, groundwater has been exploited at a rate higher than the natural recharge rate, leading to depletion of fresh groundwater resources [*Famiglietti et al.*, 2011]. At present, groundwater recharge is enhanced by managed aquifer recharge (MAR) to replenish overdrafted aquifers and utilize the storage capacity [*Bouwer*, 2002; *Massmann and Sültenfuß*, 2008]. For optimal use and protection of groundwater, knowledge of the key characteristics of the groundwater system, such as recharge locations and mechanisms, groundwater flow patterns and subsurface residence times, are essential.

The Groundwater Ambient Monitoring and Assessment (GAMA) program [*Belitz et al.*, 2003; *Belitz et al.*, 2010] aims to assess the state and development of groundwater resources in California. A large proportion of the monitoring effort is dedicated to the collection and analysis of groundwater quality samples [*Deeds et al.*, 2012; *Fram and Belitz*, 2011a; b; *Jurgens et al.*, 2009; *Landon et al.*, 2011]. Simultaneous collection and analysis of environmental tracers, including tritium, stable isotopes of the water molecule and dissolved noble gases and the helium isotope ratio, has created a large database containing valuable information regarding key groundwater characteristics, that allows assessment of contamination vulnerability and sustainability of groundwater abstraction.

Tritium is a qualitative tracer for modern groundwater that has recharged since the start of the nuclear era in 1945 [*Nir*, 1964; *Vogel et al.*, 1974]. Combined with the analysis of helium-3, the age of groundwater recharged after about 1950 can be calculated from the ratio of tritium and its decay product [*Poreda et al.*, 1988; *P. Schlosser et al.*, 1988; *Takaoka and Mizutani*, 1987]. Accumulation of helium-4 in groundwater, from the decay of naturally occurring uranium and thorium, provides a qualitative age tracer in the 500 year to million year time scale [*Peter Schlosser et al.*, 1989; *D K Solomon et al.*, 1996]. Dissolved noble gas concentrations in groundwater reflect the climatic and hydrological conditions at the time of recharge, such as temperature and water table fluctuations [*Aeschbach-Hertig et al.*, 2000; *Stute et al.*, 1995; *Stute et al.*, 1992; *Wilson and McNeill*, 1997]. Stable isotopes of the water molecule, deuterium and oxygen-18, vary spatially in precipitation in California due to continental and orographic effects [*Kendall and Coplen*, 2001]. The stable isotope signature in groundwater acts as a fingerprint of the origin of precipitation if recharge occurs aerially or by river bank filtration downstream of the source area. These analyses, taken together and interpreted in a physiographic context, allow us to address the following questions:

- Where are young groundwater ages found, indicating areas of active recharge?
- Which aquifers contain modern groundwater that is vulnerable to surface contamination?
- Where is pre-modern or fossil groundwater abstracted and over what time scale is the abstraction sustainable considering the reservoir volume and the rates of recharge and abstraction?
- Does managed aquifer recharge leave distinguishable isotopic signatures that can be used to trace its footprint and efficacy?
- Do recharge conditions reflect mean annual climate? Which processes can explain the differences between noble gas derived climate reconstruction and the observed climate conditions?
- Have recharge conditions changed since the beginning of the modern era and the intensification of the water cycle?

To answer these questions, the data set of noble gas and isotopic analyses was subjected to geostatistical analysis. The spatial correlation structure of the data was analyzed and the variables of interest were mapped by means of kriging prediction based on the measured values and derived parameters. The geostatistical analyses were performed on the state-wide data set, which was divided into subsets according to depth or age in order to address specific questions, as well as on a regional basis to investigate individual groundwater basins.

2 METHODS

2.1 Study Area

The state of California covers 424 thousand square kilometers between 33 and 42 degrees North latitude on the west coast of the United States. Physiographic features include the Coastal Range, the Central Valley, the Sierra Nevada and Cascade mountain ranges and the Mojave Desert. Elevation (Figure 1a) varies from below sea level in Death Valley and the San Joaquin-Sacramento Delta to 4421 m above sea level on top of Mt Whitney. The large latitudinal and elevational span leads to a wide range in mean annual air temperatures, from 2°C in the Sierra Nevada to 24°C in the Mojave Desert (Figure 1d). A spatial coverage of the average air temperature on a 0.25 degree resolution grid was obtained from BerkeleyEarth.org [*BerkeleyEarth.org*, 2013]. Central California has a Mediterranean climate and, as a consequence, precipitation occurs during winter and early spring [*Lundquist et al.*, 2005]. The spatial distribution of precipitation (Figure 1b), obtained from NationalAtlas.gov, ranges from less than 100 mm in the southeast to over 3000 mm in the northwest. Nearly 80% of precipitation in the Sierra Nevada is deposited as snow [*Natural Resources Conservation Service*, 2013]. Snowmelt is drained from the Cascade Range and Sierra Nevada by rivers like the Sacramento, Tuolumne, Kings and Kern River, experiencing peak flow in late spring [*Lundquist et al.*, 2005]. While most rivers are dammed, reservoir capacity is insufficient to capture peak flow entirely. Groundwater basins [*Department of Water Resources*, 2003] cover about 170 thousand square kilometers of land surface, mostly in the Central Valley (Figure 1c). The Mediterranean climate and snowmelt discharge cause natural recharge of groundwater to occur seasonally. Additional recharge comes from irrigation return flow, making up the majority of recharge in intensively farmed regions such as the southern Central Valley and the Salinas Valley.

Water districts in highly populated areas with little precipitation employ managed aquifer recharge operations to replenish aquifer reserves, using storm water runoff, imported water or treated wastewater. While dams, reservoirs and canals control most surface water flows, abstraction, irrigation and artificial recharge dictate groundwater flow patterns over much of the state. As such, California groundwater systems are part of the anthropogenic hydrological cycle. As a result, patterns of isotopic and noble gas signatures are expected to have changed since the pre-modern era.

2.2 Data Collection

The data analyzed here were collected as part of a number of large and small research projects. The majority of the samples was collected by USGS staff as part of the GAMA Priority Basin monitoring program [*Belitz et al.*, 2003](http://ca.water.usgs.gov/gama/). The Priority Basin program applied well selection on an irregular grid, to provide a spatially unbiased data set. The Priority Basin data set was supplemented with localized studies of groundwater systems, collected by LLNL and local water district staff, as part of the California Aquifer Susceptibility (CAS) program [*Carle et al.*, 2006; *Eaton et al.*, 2003; *Moran et al.*, 2005a; *Moran and Halliwell*, 2002; *Moran and Halliwell*, 2003; *Moran et al.*, 2002a; *Moran et al.*, 2004; 2005b; *Moran et al.*, 2002b; *Moran et al.*, 2005c] and GAMA Special Studies [*McNab Jr et al.*, 2010; *McNab et al.*, 2007; *Moran et al.*, 2011; *Moran et al.*, 2009; *M. J. Singleton et al.*, 2007; *Michael J. Singleton and Moran*, 2010; *Michael J. Singleton et al.*, 2010; *Visser et al.*, 2012].

Samples were collected for tritium in 1 L glass bottles. Tritium analyses were performed at LLNL by helium-3 accumulation [*Clarke et al.*, 1976; *Surano et al.*, 1992] and at the USGS in Menlo Park by enriched liquid scintillation counting [*Thatcher et al.*, 1977]. Both techniques are capable of achieving a detection limit of 1 pCi/L (0.3 TU) and have a typical accuracy of 5%.
Noble gas and helium isotope samples were collected in 10 mL copper tubes and were analyzed at the LLNL noble gas mass spectrometry facility [*Cey et al.*, 2008; *Rademacher et al.*, 2001; *Visser et al.*, 2013b]. Measurement uncertainty of the helium isotope ratio and dissolved concentrations of helium, neon, and argon is 2%; and uncertainty is 3% for krypton and xenon concentrations. The total number of analyses is presented in Table 1.

2.3 Data Reduction

Noble gas derived parameters (recharge temperature, excess air, terrigenic helium-4, terrigenic helium isotope ratio and tritiogenic helium-3) were calculated using the unfractionated excess air (UA) model [*Heaton and Vogel*, 1981]. This single, simplest excess air model was used in order to avoid bias in derived parameters resulting from the choice of the excess air model [*Visser et al.*, 2014]. The recharge elevation was assumed to be the well head elevation, extracted from the digital elevation model. The two free parameters of the UA model (noble gas recharge temperature (NGT) and excess air (EA, expressed as $\Delta Ne = (Ne_{sample}/Ne_{equilibrium} - 1)\times 100\%$) were estimated by minimizing the uncertainty-weighted squared differences between modeled and observed concentrations [*Ballentine and Hall*, 1999], denoted by χ^2 (Eq. 1), using a bound constrained quasi-Newton method [*Byrd et al.*, 1995]. $C_{i,m}$ are the modeled noble gas concentrations; $C_{i,o}$ and σ^2_i are the observed noble gas concentrations and their uncertainties.

$$\chi^2 = \sum_i \frac{(C_{i,o} - C_{i,m})^2}{\sigma_i^2} \quad \text{(i=Ne, Ar, Kr, Xe)} \qquad \text{[Eq. 1]}$$

The probability of the model parameters was obtained from the χ^2 distribution if the degrees of freedom were greater than zero [*Johnson et al.*, 1995]. The χ^2 distribution has an expected value equal to the number of degrees of freedom. Parameter sets with a χ^2 probability ($P\chi^2$) of less than 1% were rejected. The UA model was initially fitted to the dissolved concentrations of all five noble gases, including helium, leaving 3 degrees of freedom. Samples containing terrigenic helium yielded large χ^2 values resulting in low parameter probability. The UA model was then fitted to the dissolved concentrations of the four atmospheric noble gases (Ne, Ar, Kr, Xe), leaving 2 degrees of freedom. If no acceptable fit was obtained, the UA model was fitted to all 4 combinations of 3 atmospheric noble gases. The parameter set with the highest probability was selected, if it exceeded 1%. The UA model was fitted successfully to 3743 samples (Table 1).
The propagated uncertainty of the estimated parameters (NGT and EA) was calculated according to Ballentine and Hall [1999]. For approximately 300 samples, no acceptable fit was obtained. For the calculation of terrigenic and tritiogenic helium components in these samples, the recharge temperature was assumed to be equal to the mean annual air temperature. Excess air amount was derived from the measured neon concentration in these samples. The terrigenic helium concentration and isotope ratio and tritiogenic helium component were calculated after subtracting the atmospheric helium components derived from the neon excess air amount.

2.4 Groundwater Age Calculation

For samples without significant terrigenic helium-4 (< 2×10^{-9} cm3STP/g, n=1947), the tritiogenic helium concentration ($^3He_{trit,He}$) is calculated from the measured sample helium isotope ratio (R_s) and concentration (He_s), the atmospheric helium isotope ratio ($R_a = 1.384 \times 10^{-6}$), the equilibrium helium concentration ($^4He_{eq}$) and the helium isotope dissolution fractionation factor ($\alpha = 0.983$, Eq. 2).

$$^3He_{trit} = (R_s - R_a) \times {}^4He_s + (1 - \alpha) \times R_a \times {}^4He_{eq} \qquad \text{[Eq. 2]}$$

The uncertainty associated with the tritiogenic helium is derived from the measurement uncertainties of the measured helium isotope ratio and helium concentration, assuming these are uncorrelated, and the uncertainty of the equilibrium helium concentration:

$$\sigma_{3Hetrit} = \{ [(R_s - R_a) \times \sigma_{4Hes}]^2 + [\sigma_{Rs} \times {}^4He_s]^2 + [\sigma_{4Hes} \times \sigma_{Rs}]^2 + [(1 - \alpha) \times R_a \times \sigma_{4Heeq}]^2 \}^{½} \qquad \text{[Eq. 3]}$$

Terrigenic helium-4 ($^4He_{ter}$, Eq. 4) and non-atmospheric helium-3 ($^3He_{na}$, terrigenic + tritiogenic) (Eq. 5) were calculated from the measured helium isotope ratio, the measured helium concentration and the modeled atmospheric (equilibrium and excess air) helium components (He_a). Associated uncertainties with measured and modeled concentrations were propagated accordingly.

$$^4He_{ter} = {}^4He_s - {}^4He_a \qquad \text{[Eq. 4]}$$

$$^3He_{na} = {}^3He_{ter} + {}^3He_{trit} = {}^3He_s - {}^3He_a \qquad \text{[Eq. 5]}$$

For samples containing terrigenic helium, the tritiogenic and terrigenic helium-3 components need to be separated. A critical variable is the local terrigenic helium isotope ratio (R_{ter}), which can vary over three orders of magnitude, from radiogenic ($R_{rad} = 2 \times 10^{-8}$) to mantle derived ($R_{man} = 1 \times 10^{-5}$). (Locations where mantle helium is found in groundwater often coincide with locations where significant radiogenic helium has accumulated.) The local terrigenic helium isotope ratio was derived from a geostatistical analysis and interpolation (Section 2.5). First, the maximum tritiogenic helium-3 component was calculated (Eq. 6) under the assumption that all tritium measured in the sample originated from the initial test period (1953). The maximum tritiogenic helium-3 component was subtracted from the non-atmospheric helium-3 component to calculate the non-atmospheric tritiogenic-corrected helium-3 component (Eq. 7), which was divided by the terrigenic helium-4 concentration to derive a representative terrigenic helium isotope ratio (Eq. 8):

$$^3He_{trit,max} = {}^3H \times (e^{[\lambda \times (ts - 1953)]} - 1) \quad \text{[Eq. 6]}$$

$$^3He_{na,tc} = {}^3He_{na} - {}^3He_{trit,max} \quad \text{[Eq. 7]}$$

$$R_{ter} = {}^3He_{na,tc} / {}^4He_{ter} \quad \text{[Eq. 8]}$$

To incorporate the uncertainty in the age of the tritium, the uncertainty of the maximum tritium component was set equal to the tritiogenic-corrected ^{3}He value (Eq. 9), and integrated into the uncertainty calculation of the terrigenic helium isotope ratio (Eq. 10 and 11).

$$\sigma_{3Hetc} = {}^3He_{tc} \quad \text{[Eq. 9]}$$

$$\sigma_{3Henа,tc} = (\sigma_{3Henа}{}^2 + \sigma_{3Hetc}{}^2)^{½} \quad \text{[Eq. 10]}$$

$$\sigma_{Rter} = R_{ter} \times [(\sigma_{3Henа,tc} / {}^3He_{na,tc})^2 + (\sigma_{4Heter} / {}^4He_{ter})^2]^{½} \quad \text{[Eq. 11]}$$

The impact of the tritiogenic correction on the uncertainty of the terrigenic helium isotope estimate depends on the concentrations of tritium and terrigenic helium. For samples with a large terrigenic helium component, the tritiogenic correction is negligible. For the geostatistical analysis, only samples which contained a significant component of terrigenic helium ($^4He_{ter} \geq 1.645 \times \sigma_{4Heter}$, n=1890) and with a propagated uncertainty of the terrigenic helium isotope ratio of less than 10% of the estimated value plus the atmospheric helium isotope ratio ($Ra = 1.384 \times 10^{-6}$) were included. 897 samples were thus included in the analysis. Because of the high variability between terrigenic helium isotope ratios in regions impacted by mantle helium (e.g. northern volcanic provinces, areas in proximity to major faults), the geostatistical analysis was performed for each groundwater province separately on the 10-base logarithm of the terrigenic helium isotope ratio.

The local terrigenic helium isotope ratio ($R_{ter,loc}$) was predicted for each sample location using kriging. To avoid circular logic (prediction based on previous assumptions), the sample location for which the prediction was made was excluded from the data upon which the kriging prediction was based, in a process known as cross-validation. The cross-validation process results in residuals between the cross-validated kriging predictions and the calculated terrigenic helium isotope ratio. The root mean square error of residuals was used as the uncertainty of the local terrigenic helium isotope ratio, for each of the groundwater provinces separately, for further propagation in the $^3H/^3He$ age uncertainty.

Tritiogenic helium was then calculated by subtracting atmospheric and terrigenic components from the measured helium concentration (Eq. 12), and the uncertainty in the underlying estimates was propagated (Eq. 13).

$$^3He_{trit} = {}^3He_s - {}^3He_m - R_{ter,loc} \times {}^4He_{ter} \quad \text{[Eq. 12]}$$

$$\sigma_{3Hetrit} = (\sigma^2_{3Hes} + \sigma^2_{3Hem} + (\sigma_{Rter,loc} \times {}^4He_{ter})^2 + (R_{rad} \times \sigma_{4Heter})^2)^{½} \quad \text{[Eq. 13]}$$

Negative estimates of terrigenic and tritiogenic helium were set to zero. From the measured tritium concentration and estimated tritiogenic helium-3 concentration, the tritium-helium age was calculated given the decay constant of ^3H ($\lambda = \ln(2)/\tau_{½} = 0.05626$) (Eq. 14):

$$\tau = \ln(1 + [^3He_{trit}] / [^3H])\, \lambda^{-1} \quad \text{[Eq. 14]}$$

The uncertainty of the apparent $^3H/^3He$ age (σ_τ) depends on the analytical precision of the ^3H measurement (σ_{3H}) and uncertainty of the tritiogenic ^3He component ($\sigma_{3Hetrit}$) derived from the propagation of the noble gas measurement uncertainty [*D K Solomon et al.*, 1993]. A linear approximation of the age uncertainty is given by Eq. 15.

$$\sigma_\tau = \lambda^{-1} ([^3H] + [^3He_{trit}])^{-1} (\sigma_{3Hetrit}{}^2 + ([^3He_{trit}]/[^3H])^2 \sigma_{3H}{}^2)^{½} \quad \text{[Eq. 15]}$$

Samples containing less than 1 pCi/L of tritium (n=977, Table 2) must have recharged before the start of atmospheric testing of nuclear fission devices (1950) and were assigned an age of 60 years for the purposes of binning the age data (see [*Visser et al.*, 2013a] for a discussion of 'tritium dead' results for a subset of this data set). Two acceptance criteria (Table 3) were evaluated for the calculated $^3H/^3He$ ages: (1) the calculated recharge year must be after 1950 and (2) the propagated uncertainty must be less than 5 years plus 10% of the estimated age. $^3H/^3He$ ages that corresponded to a recharge year before 1950 were discarded (n=221). Tritium-helium ages with an associated uncertainty of more than 5 years plus 10% of the estimated age (n=718) were also discarded. In total, 1630 $^3H/^3He$ ages were accepted, in addition to 977 samples with less than 1 pCi/L that were assigned an age of 60 years. The influence of terrigenic helium on the ability to calculate an acceptable $^3H/^3He$ age using these criteria (Table 4) is demonstrated by comparing the acceptance rate of samples with terrigenic helium (216/996 = 22%) to that of samples without terrigenic helium (1414/1573 = 90%).

2.5 Geostatistical analysis

To create maps of noble gas derived parameters and groundwater age, the spatial structure of the data was analyzed geostatistically, in particular by kriging, using the gstat package [*Pebesma*, 2004] of the statistical software R [*Bivand et al.*, 2013; *R Core Team*, 2013]. Prior to the analysis, the statistical distribution of the data was evaluated by histogram analysis and a Shapiro-Wilks test for normality [*Shapiro and Francia*, 1972]. While the distributions of all variables in the data set were significantly different from normal, the distributions of tritium, terrigenic helium and excess air were visibly skewed. A log-transformation was applied to these variables before analysis, and predicted values were back-transformed. The detection limit of tritium causes a high number of data points to occur at the 1 pCi/L level and the distribution of the log-transformed tritium concentration lacks a

left tail. Regardless of the non-normal distribution of the data sets, variogram analysis and kriging prediction were applied.

For each variable (*Z*), the variogram (γ) was calculated from all sample pairs with lag distance *h* between locations (*s*) as:

$$\gamma(h) = ½\ \mathrm{E}(Z(s) - Z(s+h))^2 \qquad \text{[Eq. 16]}$$

under the assumption that the spatial correlation of Z does not depend on location s, but only on separation distance h. Under the assumption of isotropy (i.e., the correlation does not depend on the direction of the lag distance), the sample variogram $\hat{\gamma}$ was estimated from N_h sample pairs for binned distance intervals $\tilde{h}_j$:

$$\hat{\gamma}(\tilde{h}_j) = \frac{1}{2N_h}\sum_{i=1}^{N_h}(Z(s_i) - Z(s_i + h))^2, \forall h \in \tilde{h}_j \qquad \text{[Eq. 17]}$$

For state-wide geostatistical analyses, the bin width was 10 km. A spherical variogram model (Eq. 18) defined by the nugget *n*, the partial sill *s*, and the range *r*, was fitted to the sample variogram for each variable. Variogram analysis was performed on the entire data set for each variable, as well as on subsets of the data.

$$\gamma(h) = \begin{cases} n + s\left(\dfrac{3h}{2r} - \dfrac{h^3}{2r^3}\right) & 0 < h < r \\ n + s & h \geq r \end{cases} \qquad \text{[Eq. 18]}$$

Figure 2 shows an example variogram. Blue circles represent the distance-binned Sample Variogram. The Sample Variogram is represented by a Spherical Variogram Model (blue line). The parameters of the Spherical Variogram Model are (in this case) a nugget *n* of 0.25, a range *r* of 100 km and a partial sill *s* of 0.5. The total variance in the data is the sum of the nugget and partial sill (0.75). This variogram shows that variance between samples collected is very close to one third (0.25/0.75) of the variance of the entire data set, due to the spatial correlation. The variance of a set of samples collected at greater distances increases, as the spatial correlation decreases. Samples collected more than 100 km apart are no longer correlated.

Maps of variables were obtained by ordinary kriging prediction, yielding linear unbiased predictions of variables at gridded locations, at a 0.005 degree resolution for the statewide maps, corresponding to distances of 0.5 km. After prediction, log-transformed variables were back transformed. Variables controlled by climate or precipitation (noble gas recharge temperature and stable isotope composition) were predicted for the entire California land surface area. Variables related to groundwater properties (e.g. tritium concentration, age) were predicted only for grid cells within a DWR-defined groundwater basin. It should be noted that the kriging prediction does not include a spatial connectivity analysis. Samples in disconnected groundwater basins can therefore impact predictions across groundwater divides.

2.6 Depth Evaluation

All geostatistical analyses are initially performed in two horizontal dimensions. To investigate the vertical age stratification and the depth of modern groundwater penetration, the tritium and terrigenic helium data sets were split into three depth categories, based on the top of the well screen. The top of the screen was chosen (as opposed to the bottom or center) as an indicator of the depth of the boundary between modern and pre-modern because modern groundwater generally overlies pre-modern groundwater. (The bottom of a screen in a well producing tritium can be far below the boundary between modern and pre-modern groundwater if the tritiated water enters the well at the top of the screen.) Screen depth thresholds were chosen at 200 ft and 400 ft, resulting in nearly equally sized data sets. However, the statistical distribution of data in each subset was distinctly different, because the proportion of pre-modern groundwater was larger at greater depths. Also, the spatial distribution of wells within each category was no longer unbiased. The subsets were subject to geostatistical analysis and kriging prediction to create depth specific maps of these two tracers. In addition, the depth to tritium-free pre-modern groundwater was mapped. The geostatistical analysis was performed on the log-transformed depth to the top of the screen of all tritium-free groundwater wells. The top of the screen is only an indication of the depth to the boundary between modern and pre-modern groundwater. The top of a well screen may be far below the actual boundary depth, possibly leading to an over-estimation of the boundary depth. Tritium-free groundwater may be found at shallower depths, but go unnoticed if no shallower wells exist that do not abstract tritiated groundwater from above the boundary.

3 RESULTS

3.1 Tritium and Groundwater Age

Two variables related to age of the modern groundwater component were investigated: tritium concentration and the $^{3}H/^{3}He$ age. The spatial correlation length of the log-transformed tritium concentrations and the $^{3}H/^{3}He$ age , derived from the variograms, is 110 and 79 km, respectively (Figure 3 and 4). The short lag variability (nugget effect) constitutes about half of the total variation. The variograms were fitted to a spherical model (Table 5).

Maps of tritium concentrations (Figure 3) and groundwater age (Figure 4) show that high tritium concentrations are generally found in areas with young groundwater ages. This is especially visible in the Central Valley. The tritium concentrations in these samples are therefore largely determined by the mixing of pre-modern (^{3}H free) groundwater with modern groundwater (containing ^{3}H) and not by decay of atmospheric tritium. In contrast, in samples from short-screened monitoring wells with a distinct age, high concentrations of tritium are found in older modern groundwater, as a result of high initial tritium concentrations in water that recharged in the 1960's and 1970's, which contains bomb-pulse tritium. The areas with the youngest groundwater ages, like the northwestern coast and the upper Los Angeles basin, have moderately low (1-10 pCi/L) tritium concentrations.

Young $^{3}H/^{3}He$ ages delineate the locations of groundwater recharge. These are found in particular in the following areas:

- South San Joaquin Valley, near the Kings and Kern Rivers
- Central San Joaquin Valley, near the Tuolumne, Stanislaus and Merced Rivers
- Middle Sacramento Valley
- South Santa Clara Valley Basin (forebay)
- Upper Los Angeles Basin (forebay)
- Along the Colorado River on the Arizona and Mexican borders
- Along the northern coast
- Along the eastern slopes of the Sierra Nevada

In a general sense, recharge occurring in these areas makes aquifers vulnerable to contamination from the surface.

High precipitation rates occur in northern California and in the Sierra Nevada. However, these areas have little surface alluvium to allow direct infiltration of precipitation. Regional groundwater flow patterns in the South Bay and central coastal basins, with young groundwater ages and recharge occurring in the forebay portions of the Salinas and Santa Clara valleys, are the result of managed recharge and natural infiltration of precipitation in unconfined portions of those basins. Areas with very low precipitation, like the Mojave Desert, are associated with fossil groundwater abstraction, because present day precipitation rates are insufficient to contribute to substantial recharge. At present, a number of areas with low precipitation do show young groundwater ages, indicative of modern recharge, for example along the eastern San Joaquin Valley, in the Los Angeles basin and in Owens valley. In these areas, the groundwater reservoir is recharged by surface water imports, both natural and anthropogenic. Surface water recharge occurs along rivers and unlined canals fed by Sierra Nevada snowmelt; imports and recharge of recycled wastewater occur in the Los Angeles physiographic basin via managed aquifer recharge leading to young groundwater ages [*McDermott*

et al., 2008]. Present day recharge is dominated by these forms of surface water infiltration, rather than precipitation.

3.2 Terrigenic helium concentration and isotope ratio

The spatial correlation length of the log-transformed tritium concentrations is 113 km (Figure 5). The short lag variability (nugget effect) constitutes about half of the total variation. The variogram was fitted to a spherical model (Table 5).
In general, high concentrations of terrigenic helium are found in groundwater with older $^{3}H/^{3}He$ ages, often where the assigned age is 60 years, representing tritium-dead, pre-modern groundwater, as in the Basin and Range province and the Mojave Desert, the western San Joaquin Valley, and the eastern side of the Sacramento Valley. Fossil groundwater in the Mojave Desert coincides with very low precipitation rates. Groundwater in the Mojave Desert is nearly stagnant and abstraction of fossil water risks depletion of a finite resource. The west side of the San Joaquin Valley lacks the river recharge from major, perennial rivers that occurs on the east side. Groundwater abstraction in the western San Joaquin Valley will thus draw in lateral flow from recharge occurring in the eastern San Joaquin Valley [*Bolger et al.*, 2011]. The Monterey and Santa Clara Valley and Los Angeles Basin coastal areas are down-gradient of the forebay areas of regional groundwater flow systems [*Hudson et al.*, 2002; *Moran et al.*, 2002a]. Under natural conditions, this resulted in submarine groundwater discharge. At present, abstraction of fresh water from these aquifers has led to sea water intrusion [*Werner and Simmons*, 2009].

While the concentration of terrigenic helium appears to be correlated to the residence time of the groundwater, the terrigenic helium isotope ratio is associated with faults and volcanic geology (Figure 6). As a result, the variograms vary significantly between provinces. The highest terrigenic helium isotope ratios (> 4 R_a) are found in the southern part of the San Francisco bay area, associated with the San Andreas Fault system. Another hotspot is found further south, near Gilroy. Further south along the San Andreas Fault, high helium isotope ratios are found along the Big Bend section, near Cuyama, and the along the Elsinore Fault Zone in the San Diego Temecula Study Unit. High terrigenic helium isotope ratios are also found in the volcanic areas of Sonoma-Napa Valley, the Modoc Plateau and Cascades province, and near Martis Valley. Surprisingly, large portions of the Central Valley show terrigenic helium isotope ratios far higher than the radiogenic signature. The highest observed ratios in the Central Valley are associated with Sutter Buttes [*Jenden et al.*, 1988], but mantle helium in other large areas of the northern and southeastern Central Valley cannot be explained by recent igneous activity. Terrigenic isotope ratios equivalent to radiogenic production of helium are found only in the western San Joaquin Valley, Monterey Bay, and the South Coast Basins.

3.3 Depth Evaluation

The depth to the top of the screen is available for 1919 samples. The median tritium concentrations at the three depth intervals (0-200 ft, 200-400 ft and below 400 ft) are 7.8, 3.0 and 1.6 pCi/L. Mean concentrations are higher (10.2, 7.2 and 7.3 pCi/L) due to the skewed distribution of tritium concentrations. The variogram of log ^{3}H concentrations in shallow wells (0-200 ft, Fig. 7a) has a similar shape as the variogram of all tritium data, but with a lower nugget parameter of 0.15 and a lower total variance. The variogram of intermediate wells (200-400 ft, Fig. 7b) has a lower nugget than the entire data set, but a higher total variance. The variogram of log ^{3}H concentrations in deep (Fig 7c) wells shows a very poor spatial structure with a high nugget (0.5), a short range (50 km) and

a higher total variance (0.7). The variograms for the entire dataset for each variable were therefore used to predict the depth specific maps (Figure 7a-f). Fewer data points are available in each depth interval and the effect of kriging interpolation across disconnected groundwater systems is more pronounced.

The analysis of shallow (0-200 ft) data predicts a tritium concentration of more than 3 pCi/L for the entire Central Valley. When all depths were considered, tritium free groundwater was predicted in the north west part of the San Joaquin Valley because all wells in this area had top-of-screens below 200 ft. Low tritium, long residence time groundwater in the shallow aquifer system of Sonoma County was documented previously in Moran et al. [2010]. Comparison of shallow (0-200 ft) with intermediate (200-400 ft) and deep (>400 ft) groundwater shows decreasing tritium concentrations with depth, as a result of age stratification. The depth to pre-modern groundwater, illustrated in these figures, is an important consideration because pre-modern is less likely to be affected by anthropogenic contaminants [*Fram and Belitz*, 2011a; *Visser et al.*, 2013a]. Figure 7c also shows areas where modern groundwater has reached great depths in some groundwater basins. While most aquifers contain less than 3 pCi/L tritium below 200 ft, tritium is found in wells with the top of the screen below 200 ft in Santa Clara Valley, the western San Joaquin Valley and the Los Angeles basin. Tritium concentrations above 3 pCi/L were not found in wells with the top of the screen below 400 ft, except in the Los Angeles basin. Here, intense managed aquifer recharge and deep groundwater pumping draws modern groundwater down to greater depths. Tritium concentrations somewhat higher than in surrounding areas that are found in the southern San Joaquin Valley are also likely the result of intense pumping and recharge via return flow of imported irrigation water.

Variograms of terrigenic ^{4}He concentrations in each depth category were very similar to variograms of all terrigenic helium data. Terrigenic ^{4}He shows the opposite pattern of ^{3}H, with increasing terrigenic ^{4}He found in deeper aquifers. The median concentrations of terrigenic helium in each of the depth classes are 1.5, 4.3 and 11.3×10^{-9} $cm^{3}STP/g$. Mean concentrations are higher (283, 251 and 326×10^{-7} $cm^{3}STP/g$) due to the skewed distribution of terrigenic helium concentrations. Exceptions are areas where modern water has reached deeper parts of the aquifer, as discussed above, and terrigenic helium is low or absent, even in deep-screened wells, such as in the southwestern San Joaquin Valley and LA Basin. High concentrations of terrigenic ^{4}He over all depths, as observed in the southeastern deserts and the northeastern Sacramento Valley (Fig 7d, e, f) delineate regions of low recharge and very long groundwater residence time throughout the aquifer system.

The depth to the top of the screen is available for 470 tritium-free wells. The spatial structure of the log-transformed depth to tritium free groundwater has a correlation length of 74 km. The sill and spherical component of the variogram are of equal size, indicating a significant short lag variability. The depth to tritium-free groundwater typically varies between 100 and 400 ft (Fig 8). Four areas stand out having a very deep boundary between modern and pre-modern groundwater. In the area between Woodland, Davis and Sacramento, the boundary is as deep as 500-600 ft. Two wells with depths to the top of the screen of 740 and 1260 ft pull down the estimate. The closest nearby well with a depth to the top of the screen of 258 ft contains 13.6 pCi/L tritium and nearby wells that contain over 8 pCi/L tritium have depths to the top of the screen of up to 375 ft. While the two deep screened wells may cause the map to overestimate the boundary between tritium-free and modern groundwater, tritiated groundwater is found at great depths in this area. Similar depths to tritium-free groundwater are found in the Santa Clara River Valley, San Gabriel Basin and in the Mojave Study Unit near Esperia. Tritium-free groundwater is found at shallow depths in the Volcanic

Highlands of the North San Francisco Study Unit and in the Indian Wells area of the Basin and Range province. As mentioned above, tritium-free groundwater may be present at shallower depths, but go unnoticed because shallow wells that do not also abstract tritium-bearing groundwater are not present or were not sampled.

3.4 Noble gas recharge temperature and excess air

The spatial correlation of noble gas recharge temperatures spans 175 kilometers, as expressed as the range of the spherical model (Fig 9). The short lag variability (nugget effect) equals 10.5, or nearly 60% of the total variability. The map of noble gas recharge temperatures (NGRT; Fig 9) is similar to the mean annual air temperature map (MAAT; Fig 1d). Most variation in both MAAT and NGRT is the result of the elevation gradients present in California. Noble gas recharge temperatures of up to 25 °C are found in the Mojave Desert and NGRTs below 10 °C are found in the Sierra Nevada. A latitudinal gradient along the coast trends to higher NGRT at lower latitudes, as expected. Recharge temperatures are higher in the Central Valley than at the coast at the same latitude, illustrating a continental (longitudinal) gradient related to the coastal maritime climate. High elevations in the Sierra Nevada and San Bernardino Mountains (east of Los Angeles) cause an offset in the continental temperature gradient. Because of the strong elevation gradients, local anomalies in groundwater recharge temperatures are difficult to distinguish on the map of noble gas recharge temperatures.

The spatial correlation length of the log-transformed excess air concentration spans about 100 km. The short lag variability (nugget) is more than half the total variability. The map of excess air concentrations (Fig 10) shows very high excess air concentrations in the Santa Clara Valley basin, which are a result of artificial recharge operations and recharge in incised, ephemeral creeks [*Hanson et al.*, 2004; *Moran et al.*, 2002b; *Moran et al.*, 2005c]. High excess air concentrations are also found in the San Jacinto basin. The Los Angeles groundwater basin shows a gradient of higher excess air concentrations in the forebay where artificial recharge occurs, towards lower excess air concentrations near the coast. A similar gradient is visible in the northern half of Salinas valley. The southern San Joaquin Valley, especially near Bakersfield, shows higher excess air concentrations than the rest of the Central Valley due to seasonal recharge through unlined canals [*Cey et al.*, 2008]. Low excess air concentrations are found in the Mojave Desert, where recharge rates are low and thick vadose zone dampens the groundwater table fluctuations.

3.5 Stable isotopes of water

Stable isotopes of the water molecule (with $\delta^{18}O$ as example, Fig 11) reveal a very strong spatial structure, characterized by a very small nugget (strong short lag correlation) and a long (403 km) correlation length. The steep gradient in stable isotope ratios in California caused by the ascent from the Pacific Ocean to the Sierra Nevada mountain range [*Kendall and Coplen*, 2001] results in an anisotropic spatial correlation structure. Differences between directional variograms illustrate the anisotropy in perpendicular angles of 55° and 145° from North. The anisotropy is particularly strong at distances of over 200 km. The gradients across the Sierra Nevada that are causing the anisotropy are not present throughout the state, however. The isotropic variogram was therefore used to build maps of the oxygen isotope ratio (expressed as $\delta^{18}O$). Because of the steep rise of the variogram

over relatively short distances and the spatial density of the samples, the predicted map relies more on nearby locations, where anisotropy is weakest.

The statewide map of oxygen isotope ratios show the expected pattern of the effects of evaporation and precipitation processes from a coastline across a mountain range: water enriched in the heavy isotopes – similar to the oceanic isotope signature – precipitates near the coast, while water with a lighter isotopic signature precipitates along the Sierra Nevada mountain range. Closer inspection of the $\delta^{18}O$ map reveals the effect of high elevation runoff from the Kings and Kern Rivers in the San Joaquin Valley, particularly near Fresno and Bakersfield, delivering isotopically light water with a high Sierra signature. The same effect is observed along all of the major, perennial rivers draining the Sierra Nevada, but is more subtle where the contrast is lower due to generation of the bulk of the snowmelt at somewhat lower elevation. Similarly, Colorado River water, precipitated in the Rocky Mountains, recharges near the river in the Mojave Desert and along (formerly) unlined canals carrying Colorado River water along the southern and southeastern borders of the state [*Izbicki et al.*, 2004]. Irrigation in these areas is predominately via imported surface supplies, and recharge is dominated by return flow, so the imported, high elevation isotopic signatures are distributed some distance away from the linear (river and aqueduct) features. San Bernardino valley has a similar light isotope signature, resulting from focused recharge of mountain runoff, both natural and engineered [*Kent and Landon*, 2013]. The high contrast in $\delta^{18}O$ between coastal/Central Valley and Sierra Nevada/Colorado River isotopic signatures provides a powerful tool for tracing of imported or redistributed water recharged via rivers, artificial recharge facilities, and irrigation return flow.

3.6 Regional Studies

The spatial distribution of tritium, $^{3}H/^{3}He$ age, noble gas recharge temperature and excess air (ΔNe) in three areas were studied in more detail to illustrate specific water sources and groundwater recharge processes: the San Joaquin Valley, the Santa Clara Valley and the Los Angeles Physiographic Basin. The presented maps are larger scale representations of the state-wide maps, with adjusted color scales to show smaller differences. The same limitations of the state-wide maps apply to the regional maps. The statistical distribution of the supporting data was not normally distributed, the spatial distribution of sampled wells was not even, and the applied kriging prediction technique does not distinguish between connected and disconnected groundwater basins. The latter is less relevant for these regional scale maps than for the state-wide maps.

3.6.1 San Joaquin Valley

The San Joaquin Valley was identified on the state-wide map as having distinct recharge areas in the east and an age gradient towards pre-modern groundwater on the west side (Fig 12). The general trend is more clearly visible on the tritium map, where high tritium concentrations are associated with young groundwater ages. These recharge areas coincide with distinct areas of low $\delta^{18}O$ isotope ratios, close to the signatures of the Kings River ($\delta^{18}O$ = -13.71 ‰) and the Kern River ($\delta^{18}O$ = -13.34 ‰) as described by Kendall and Coplen (2000). These isotope ratios are associated with Sierra Nevada precipitation from the highest elevations in California. The similarity of the pattern visible in stable isotope and groundwater age maps indicates that the Kern River and Kings River contribute a significant fraction of Sierra Nevada snowmelt to modern groundwater recharge, either via direct river recharge or via return flow of irrigation water from those sources. Artificial recharge activities in Fresno and Bakersfield are evidenced by higher tritium concentrations and younger groundwater

ages than surrounding areas. Recharge of Kern River water in the Bakersfield area is associated with significantly lower noble gas recharge temperatures (14.4 °C) than the mean annual air temperature (19.2 °C), and very high excess air concentrations, where unlined canals in the urban area allow fast infiltration of Kern River water.

3.6.2 Santa Clara Valley

Detailed maps of Santa Clara Valley (Fig 13) show a clear gradient of groundwater ages from the forebay area to the south towards San Francisco Bay. While young ages are associated with higher tritium concentrations on state wide maps, in Santa Clara Valley, high tritium concentrations are not associated with young groundwater ages. In this case the age gradient is more distinctive and tritium alone is not capable of identifying the flow direction. Tritium concentrations are more strongly determined by the initial tritium concentrations in specific historical recharge periods than by mixing of modern and pre-modern groundwater [*Moran et al.*, 2002a; *Moran et al.*, 2005c]. Young groundwater age and high tritium are also associated with managed aquifer recharge operations at Fremont. Relatively high tritium concentrations in the Tri-Valley area are due to historical, regulated releases of tritium from Lawrence Livermore National Laboratory. MAR operations in south San Jose result in higher noble gas temperatures (16.8 °C) than the mean annual air temperature (14.9 °C) and very high excess air concentrations (ΔNe = 198%) [*Cey et al.*, 2008]. MAR operations in Fremont are characterized by deeper recharge ponds in former gravel quarry pits that remain filled year round. As a result, the noble gas recharge temperature (14.7 °C) accurately reflects the mean annual temperature (14.7 °C). Because the saturated zone intersects the ponds, excess air formation is limited and these MAR operations result in low excess air concentrations (ΔNe = 54%).

3.6.3 Los Angeles Physiographic Basin

Detailed maps of the Los Angeles Physiographic Basin (Fig 14) highlight the patterns generated by MAR near the Anaheim Forebay and Montebello Forebay where groundwater ages in these engineered groundwater basins increase towards the coast [*Clark et al.*, 2004; *Hudson et al.*, 2002]. The pattern is interrupted by injection of large volumes of water at seawater intrusion barriers at Dominguez Gap, Alamitos Gap, and the West Coast barrier in the Los Angeles Basin and at the Talbert Gap in the Orange County Basin. Pre-modern groundwater in relatively stagnant zones prevails between areas affected by the major recharge areas in the forebay or the injection barriers [*Clark et al.*, 2004]. Comparison between tritium and the age map shows that the highest concentrations of tritium are found in groundwater with an age of 30-40 years. Here, as in Santa Clara, the tritium concentration is determined by the modern age and the initial tritium during recharge, rather than by the mixing of modern and pre-modern groundwater. Tritium analyses alone would not reveal the detail of age gradients obtained from tritium-helium analysis [*Hudson et al.*, 2002].

Recharge areas in the Los Angeles and Orange County basins, which are periodically dried and rapidly filled, are also associated with higher excess air concentrations (ΔNe = 81%) as noted by Hudson et al. [2002] and Cey et al. [2008]. Differences between the Montebello Forebay and Anaheim Forebay areas are related to the higher volume of recycled wastewater applied in Orange County compared to Los Angeles County. The recycled water imparts a higher tritium, higher recharge temperature signature in the Anaheim Forebay area.

4 DISCUSSION

Key characteristics of California groundwater systems related to aquifer vulnerability, sustainability, recharge locations and mechanisms, and anthropogenic impact on recharge are revealed in a spatial geostatistical analysis of a large data set of tritium, noble gases and isotope analyses.

The correlation length of key groundwater residence time parameters (tritium, terrigenic helium) is on the order of 100 km. The correlation length of recharge temperature is 175 km, due to the elevation dependency. The correlation length of the $\delta^{18}O$ isotope ratio is on the order of 400 km.

On the scale of California, young groundwater ages correlate with higher tritium concentrations. In some individual groundwater basins, higher tritium concentrations are associated with groundwater with ages of 30-40 years, as a result of higher historical concentrations of tritium in recharging groundwater. This distinction illustrates the differing effect on tritium concentrations between mixed groundwater samples containing a large fraction of pre-modern groundwater, and samples containing mostly modern groundwater. In mixed groundwater, the tritium concentrations are mostly determined by the fraction of pre-modern groundwater, i.e. the dilution of tritium. The tritium concentration alone is then indicative of the presence of modern groundwater, although quantification of the fraction of modern water is highly uncertain. In areas where little pre-modern groundwater is present, the tritium-helium age is essential in identifying recharge areas and flow patterns. Tritium analyses alone would point to areas where groundwater ages are 30-40 years, while $^{3}H/^{3}He$ groundwater ages delineate areas with 0-10 year old groundwater.

Regional recharge areas, indicated by young groundwater ages, are located in the eastern San Joaquin Valley, in the southern Santa Clara Valley Basin, in the upper LA basin and along unlined canals carrying Colorado River water. These areas are not characterized by higher precipitation that might result in higher infiltration and recharge. Rather, recharge in California is dominated by recharge via rivers (often controlled by reservoir releases, e.g., in the San Joaquin Valley and Colorado River system), and managed aquifer recharge (Fremont, Santa Clara Valley, Bakersfield, Los Angeles Physiographic Basin). Wells in recharge areas are most vulnerable to surface contamination [*Manning et al.*, 2005]. Managed aquifer recharge poses a smaller threat because of monitoring and regulation [*California Department of Public Health*, 2014]. Areas with young groundwater where recharge is dominated by irrigation return flow are most vulnerable. In California, these are found in the San Joaquin Valley and the upper Salinas Valley.

In the southeastern San Joaquin Valley, Santa Clara Valley and Los Angeles basin, modern groundwater is found in wells with the top of the screen below 200 ft depth. Depth alone does not protect an aquifer, especially if intensive pumping and/or managed aquifer recharge operations occur, since those activities generally decrease the time between recharge and discharge relative to the natural system. Groundwater abstracted from deep wells in the western San Joaquin Valley is somewhat more protected from surface contamination due to the presence of the Corcoran clay [*Bolger et al.*, 2011], as evidenced by observations of old groundwater ages there. The presence of pre-modern groundwater does not allow prediction of a more precise time scale of vulnerability. The available age tracer data are not capable of distinguishing groundwater ages in the 60-500 year range; however additional argon-39 analysis would potentially provide this information[*Loosli*, 1983; *Loosli et al.*, 1989]. However, modern groundwater in deeper parts of the eastern San Joaquin

Valley, affected by agricultural constituents such as salts and nitrate, will be transported laterally toward the western San Joaquin Valley, eventually threatening groundwater quality there.

Groundwater abstracted in the central Mojave Desert is mostly pre-modern and characterized as fossil water based on the presence of high concentrations of terrigenic helium. The terrigenic helium age indicates a time scale of 10-50 thousand years, based on literature assumptions of the porosity and uranium and thorium contents (Torgersen, 1980; Kulongoski et al., 2003). Modern groundwater abstracted in this area is found only near distributaries of the Colorado River, which has recharged under distinctly different conditions. This supports the notion that desert groundwater abstraction is depleting a finite resource because modern recharge with its distinct isotopic and noble gas signature has not been sampled in this region.

Managed aquifer recharge operations, intended to replenish unsustainable groundwater abstraction in the Santa Clara and Los Angeles basins, have a major impact on signatures of recharge and infiltration rates. Noble gas recharge temperatures are potential tracers for measuring the efficacy of recharge [*Cey et al.*, 2008; *D Solomon et al.*, 2010]. Noble gas signatures found under managed aquifer recharge operations are distinctly different from ambient groundwater. Differences between noble gas recharge temperature and the mean annual temperature are found where recharge occurs predominantly during one season. Surface spreading ponds recharge mostly in summer, when groundwater levels are lower due to abstraction, causing higher gradients between the pond and the aquifer and rapid recharge. Summer recharge thus results in higher noble gas temperatures than the mean annual temperature. A stable water level and infiltration through ponds deeper than the water table, typically results in very low excess air concentrations [*Massmann and Sültenfuß*, 2008; *Visser et al.*, 2012]. Examples of these effects are found in recharge operations near Fremont. Wet season (fall, winter and spring) managed aquifer recharge in spreading grounds results in lower noble gas temperature than the mean annual temperature. Sudden flooding of dry creekbeds and ponds causes high excess air concentrations, as found in the Santa Clara Valley basin (Cey et al., 2008).

Seasonal recharge also occurs naturally along rivers draining the southern Sierra Nevada, as noted above. Recharge of spring snowmelt discharge from high elevations with a distinct stable isotope signature is expressed as plumes of cold and isotopically light groundwater in the San Joaquin Valley. The mosaic of recharge and pumping under present day groundwater management practices complicates the tracing of groundwater flow paths from source to receptor. Combined analysis and application of noble gases and stable isotopes and other groundwater tracers reveal the impact of engineered groundwater recharge, and prove to be invaluable for the study of complex modern groundwater systems.

5 TABLES

Table 1: Number of analyses and derived parameters and the number of unique wells with analyses and derived parameters available.

Variable	Number of analyses	Number of unique wells
Tritium	3895	3802
- **0-200 ft deep**	1281	950
- **200-400 ft deep**	812	651
- **> 400 ft deep**	426	318
- **3H < 1 pCi/L**	977	757
- **3H ≥ 1 pCi/L**	2918	2285
Oxygen-18	4772	3445
Noble gases (EA)*	3926	3926
Noble gas model fit	3743	3743
- **He, Ne, Ar, Kr, Xe**	1288	
- **Ne, Ar, Kr, Xe**	1828	
- **Ne, Ar, Kr**	275	
- **Ne, Ar, Xe**	23	
- **Ne, Kr, Xe**	170	
- **Ar, Kr, Xe**	159	
Noble gas recharge temperature	3743	3743
Terrigenic helium	3921	3921
Terrigenic helium (significant)	1886	1499
Terrigenic helium isotope ratio	1626	1626
- **With significant terrigenic helium and an uncertainty of less than 10% Ra**	897	897
^{3}H/^{3}He age (< 60 years)	1630	1366
^{3}H/^{3}He age (incl. ^{3}H < 1 pCi/L)	2589	2141

* Number of samples for which the excess air component (EA) could be derived. EA can be derived from all atmospheric noble gases (Ne, Ar, Kr and Xe) or a subset if one or more noble gas concentrations is missing for a particular sample.

Table 2: Number of samples for which a ^{3}H/^{3}He age was calculated.

	3H < 1 pCi/L	3H ≥ 1 pCi/L	Total
No ^{3}H/^{3}He age	977	1288*	2265
^{3}H/^{3}He age	-	1630	1630
Total	977	2918	3895

* 1288 samples contain more than 1 pCi/L tritium and have no ^{3}H/^{3}He assigned, of which 349 lack location information or ^{3}He, ^{4}He or Ne measurements, and 939 were discarded because they did not meet the acceptance criteria.

Table 3: Results of the ^{3}H/^{3}He age acceptance criteria.

	Uncertainty ≤ 5y + 10%	Uncertainty > 5y + 10%	Total
Recharge year > 1950	1630*	718	2348

Recharge year ≤ 1950	87	134	221
Total	1717	852	2569

* The total number of accepted $^{3}H/^{3}He$ ages.

Table 4: Analysis of influence of terrigenic helium on acceptance criteria results.

	No $^{4}He_{ter}$	Significant $^{4}He_{ter}$	Total
Accepted $^{3}H/^{3}He$ age	1414	216	1630
$^{3}H/^{3}He$ age not accepted	159	780	939
Total	1573	996	2569

Table 5: Parameters of spherical variogram models

Variable	Nugget (*n*, Eq. 18)	Partial sill (*s*, Eq. 18)	Range (*r* (km), Eq. 18)
$^{3}H/^{3}He$ Age	261	210	79
Log_{10} tritium	0.3	0.3	110
• **0-200 ft**	0.15	0.25	110
• **200-400 ft**	0.20	0.45	90
• **> 400 ft**	0.5	0.2	50
Log_{10} terrigenic helium	0.73	0.79	113
• **0-200 ft**	0.62	0.82	119
• **200-400 ft**	0.51	1.08	108
• **> 400 ft**	0.54	0.94	151
Log_{10} terrigenic helium isotope ratio	0.01	0.48	53
Log_{10} depth to top of screen of tritium-free wells	0.039	0.042	74
$\delta^{18}O$	0.27	8.5	403
• **55°**	0	30	600
• **145°**	0.39	7.8	568
Recharge Temperature	10.5	7.5	163
Log_{10} Excess air	0.15	0.13	100

6 FIGURES

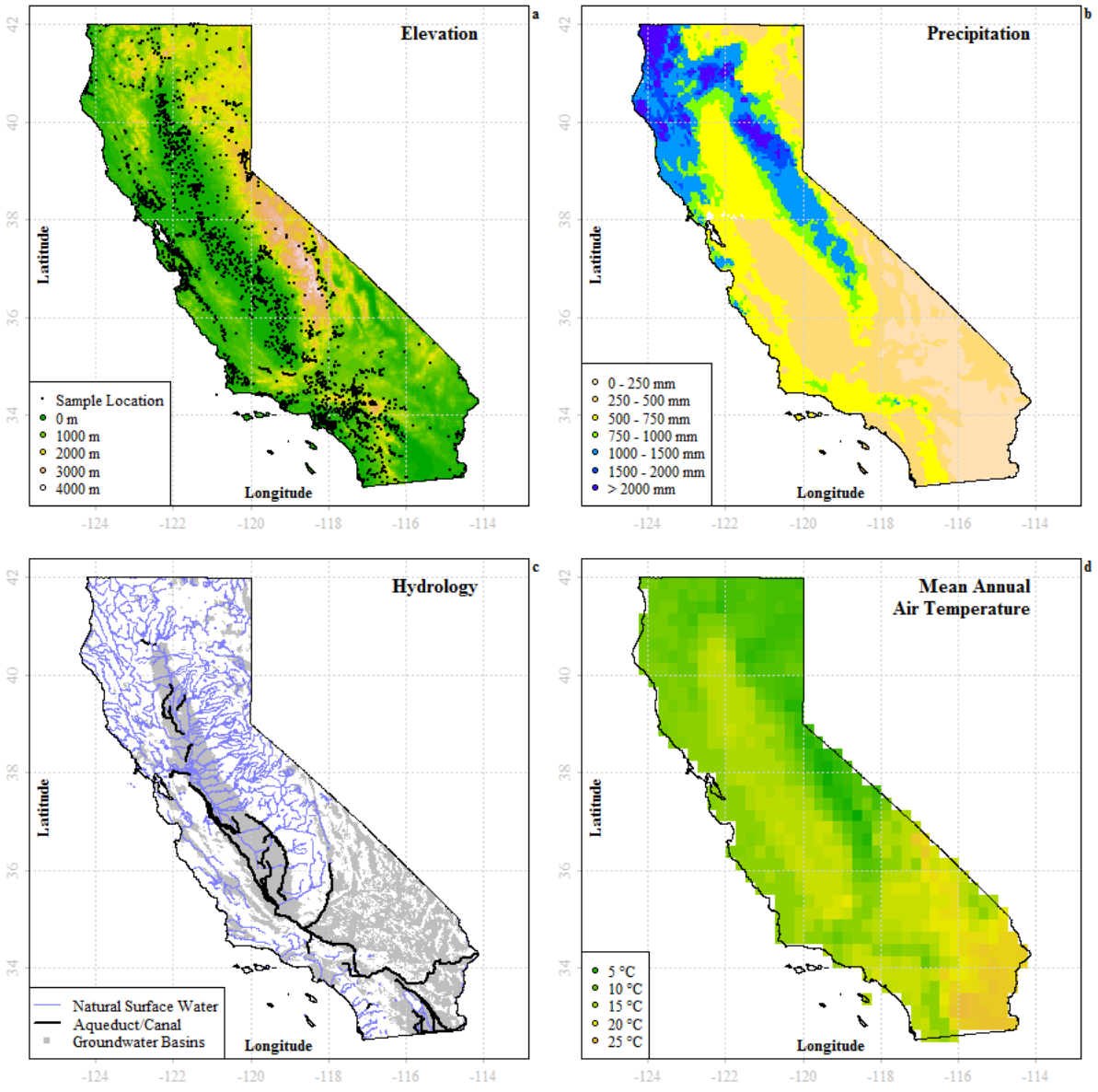

Figure 1: Maps of elevation and sample locations (a), precipitation (b), hydrology (c) and mean annual air temperature (d) in California.

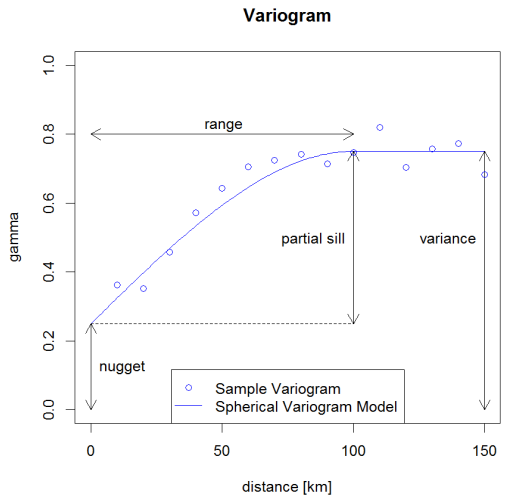

Figure 2: Example variogram, showing the nugget, partial sill and range components of the spherical variogram model.

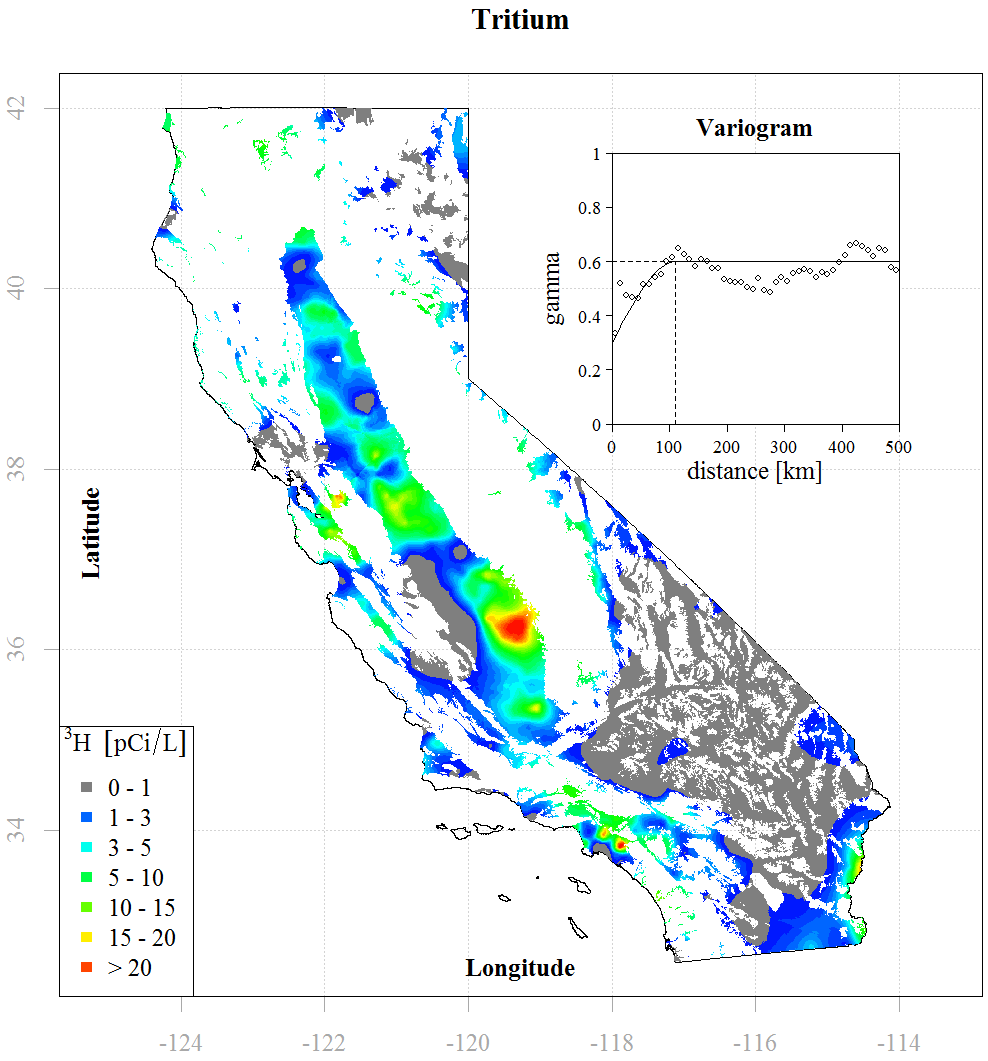

Figure 3: Predicted tritium concentrations

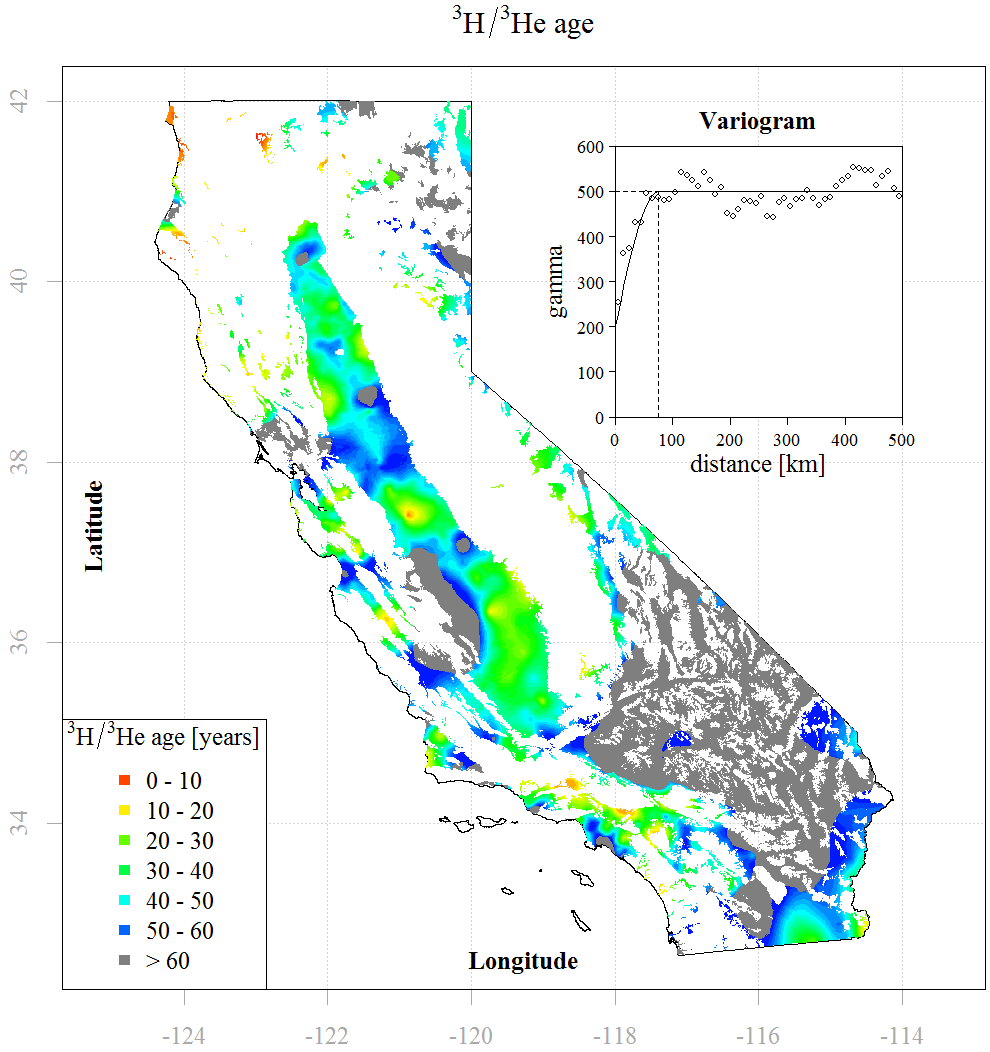

Figure 4: Predicted $^3H/^3He$ groundwater age

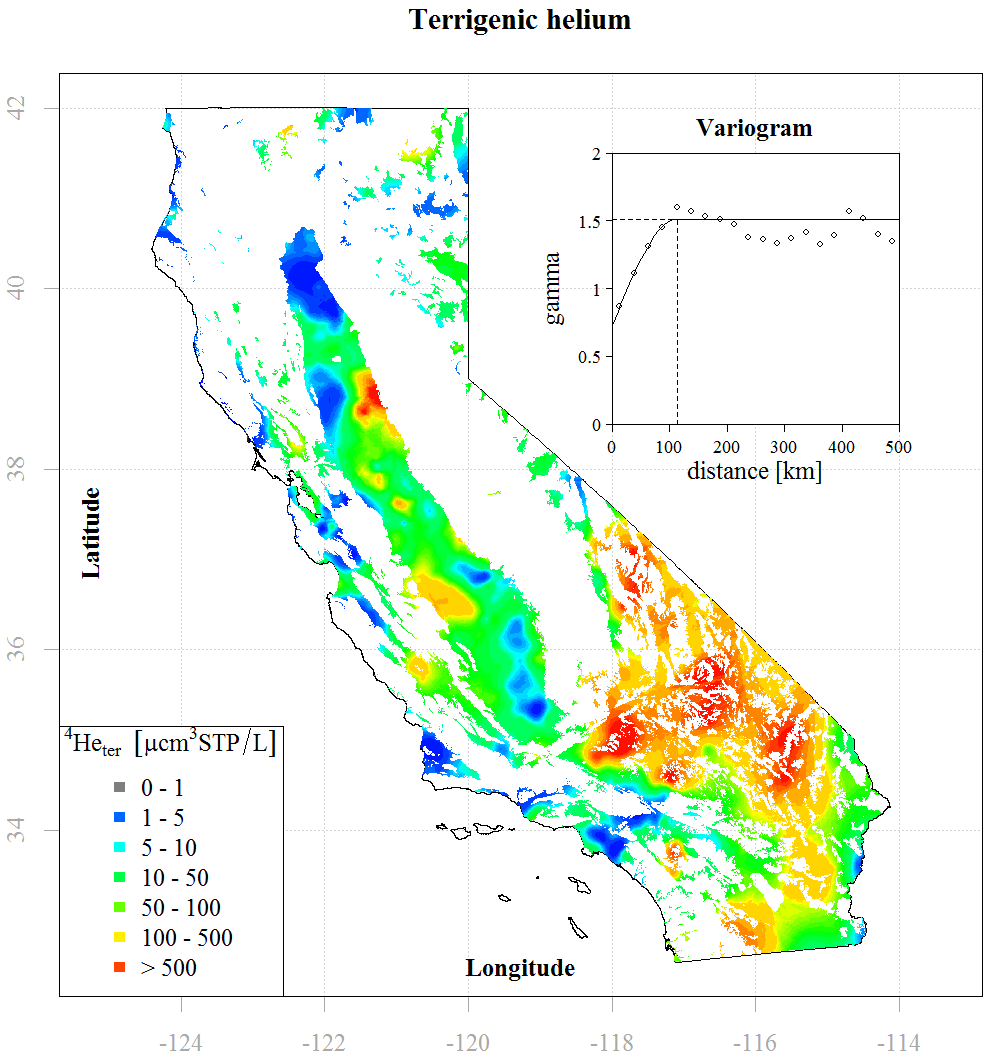

Figure 5: Predicted terrigenic helium concentration

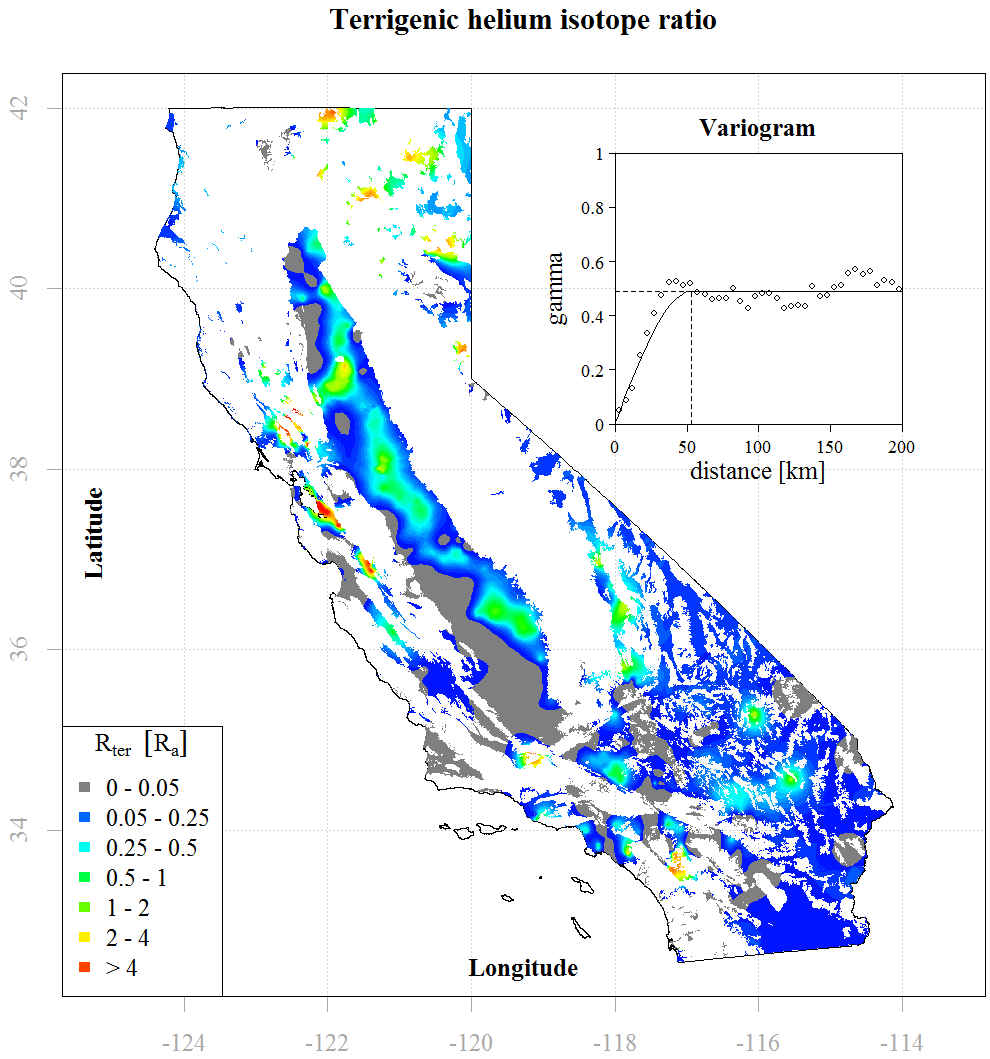

Figure 6: Predicted terrigenic helium isotope ratio (R_{ter}), relative to atmospheric (R_a).

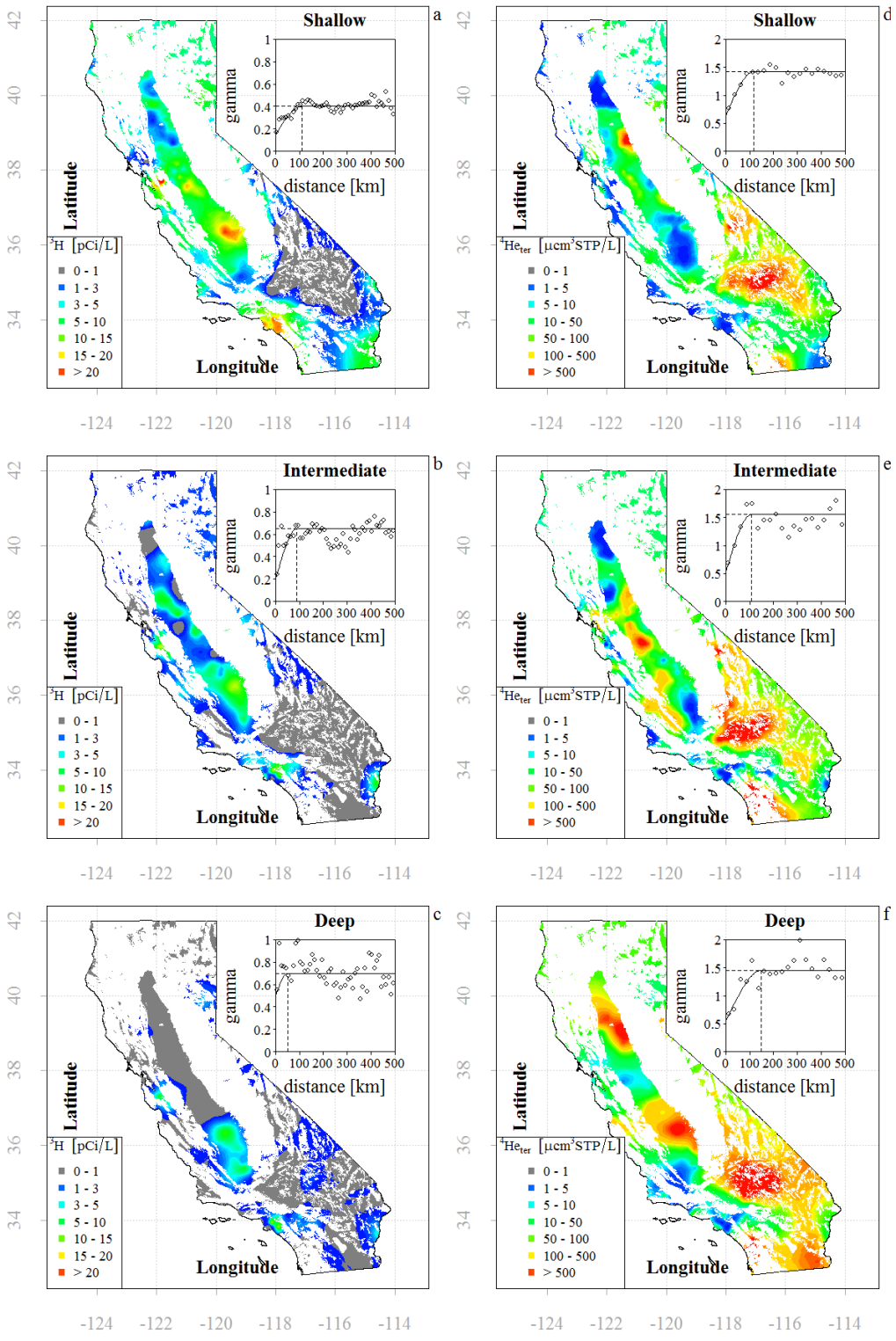

Figure 7: Predicted tritium concentrations (a, b, c) and terrigenic helium concentrations (d, e, f) for predicted for shallow (0-200 ft, a and d), intermediate (200-400 ft, b and e) and deep (over 400 ft, c and f) sections of the groundwater basins.

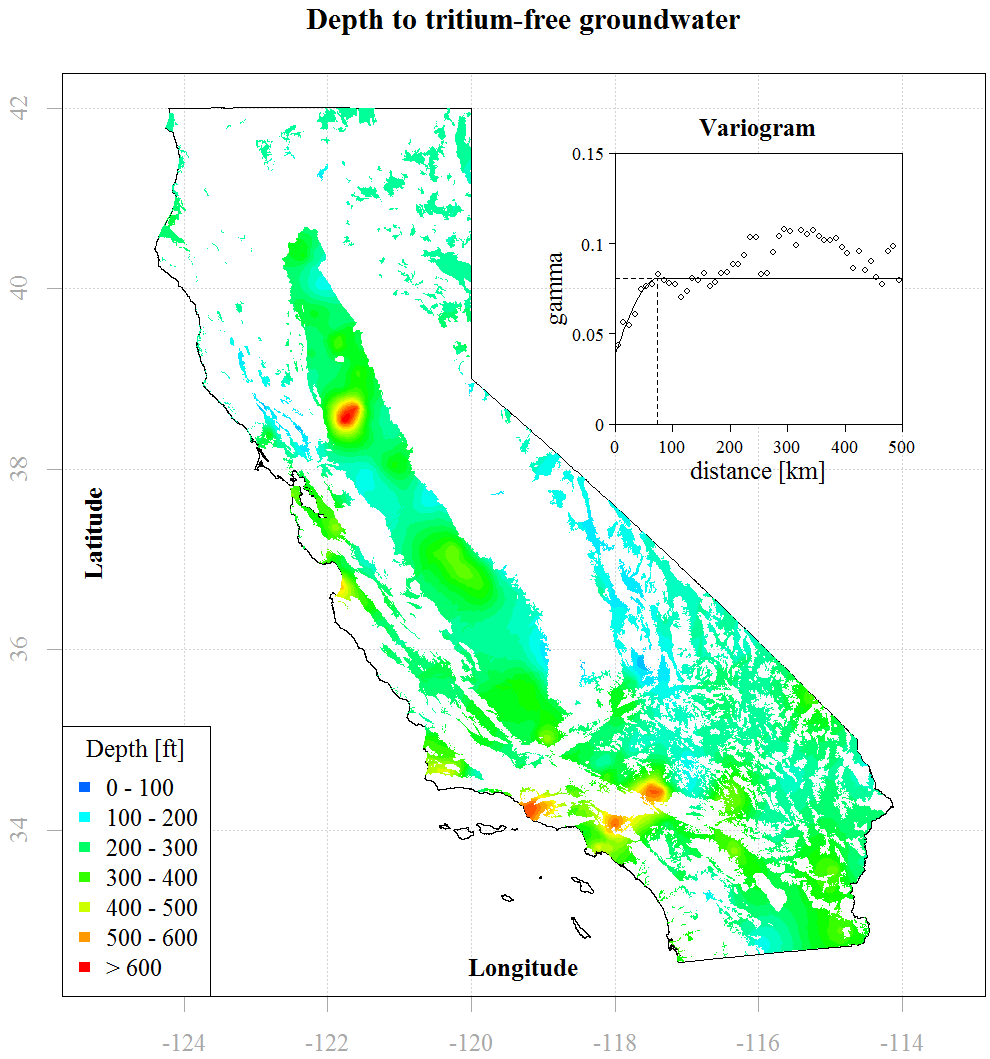

Figure 8: Predicted map of the depth to the top of the screen of tritium free groundwater wells.

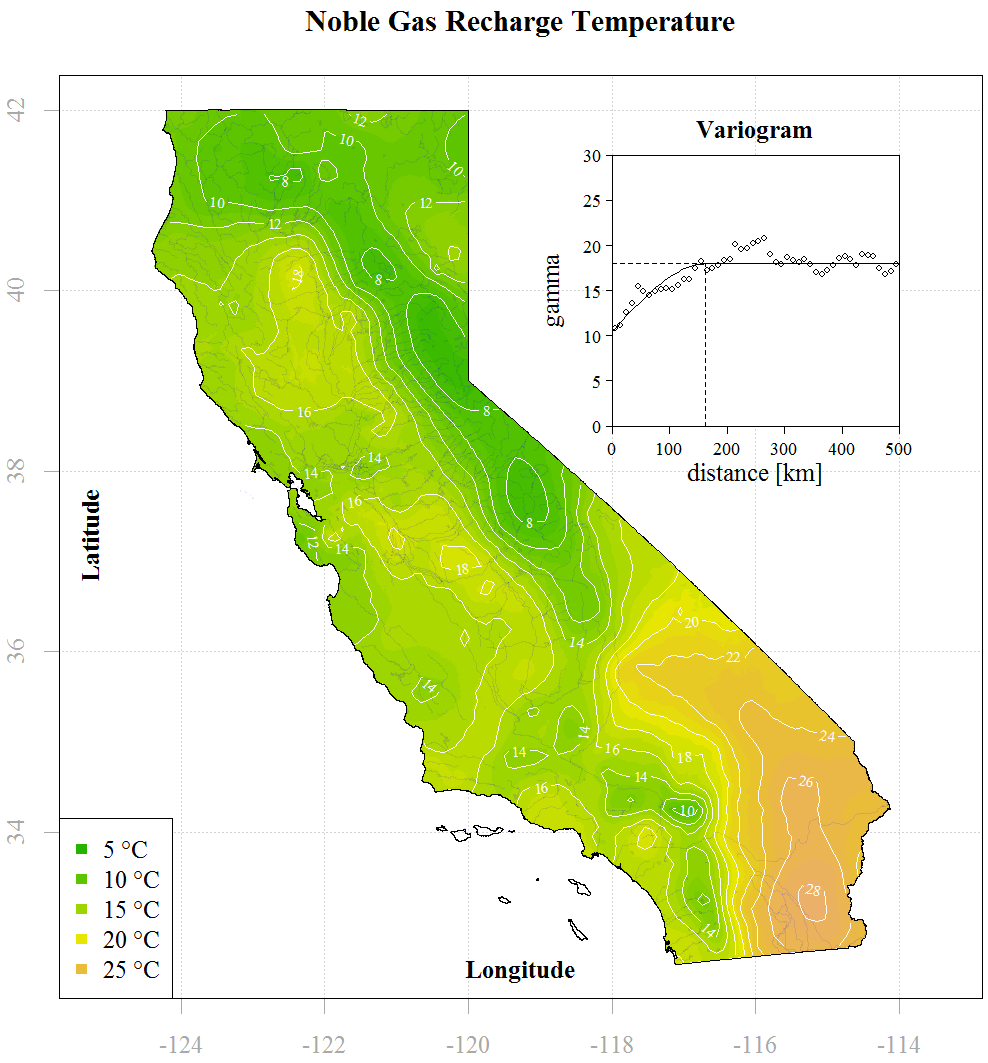

Figure 9: Predicted map of noble gas recharge temperature.

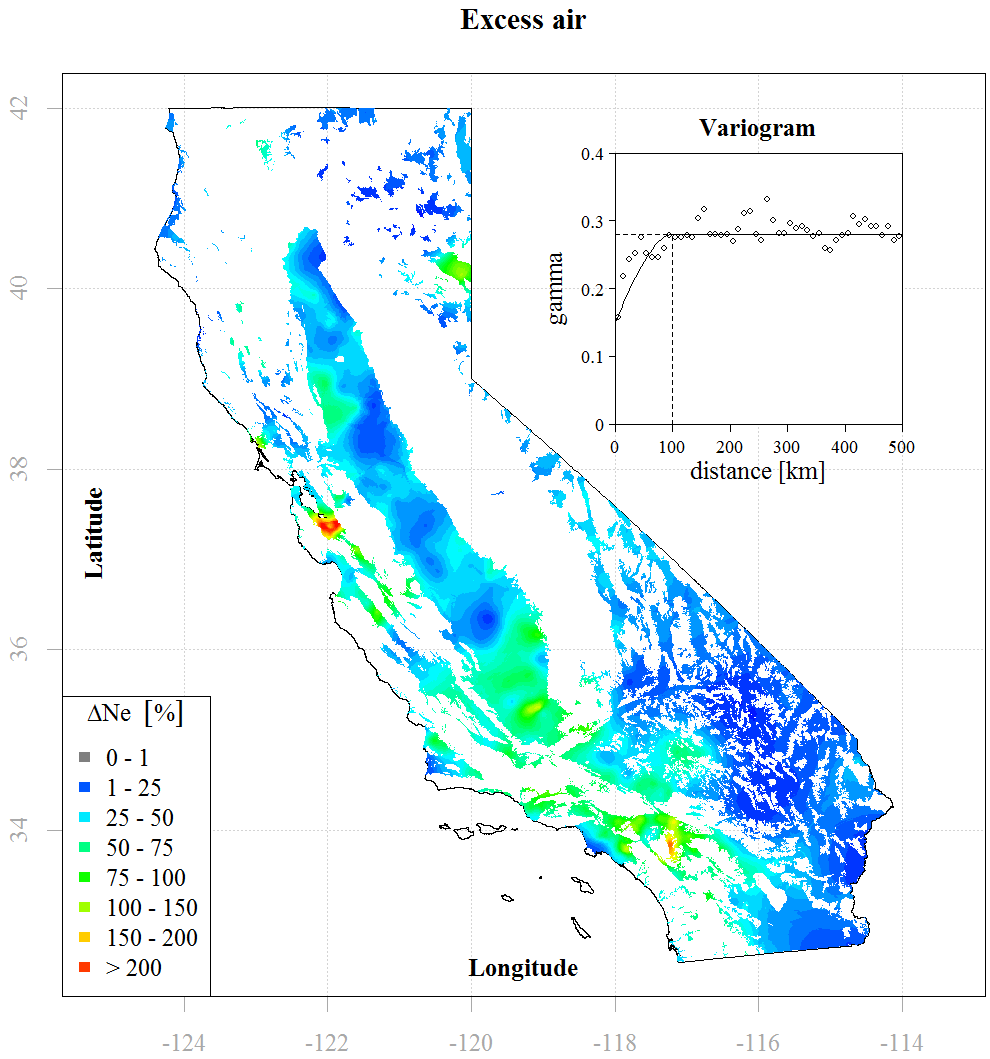

Figure 10: Predicted excess air concentration

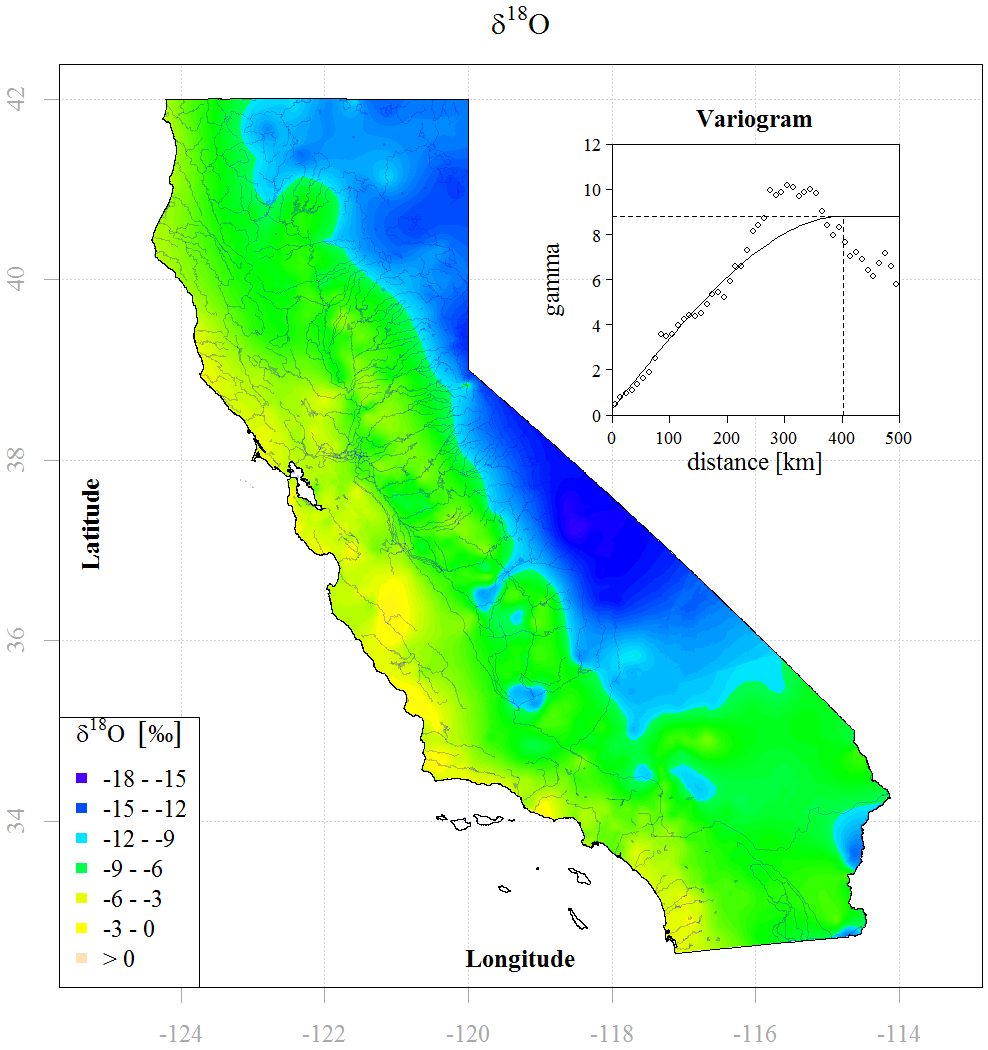

Figure 11: Predicted $\delta^{18}O$ in groundwater

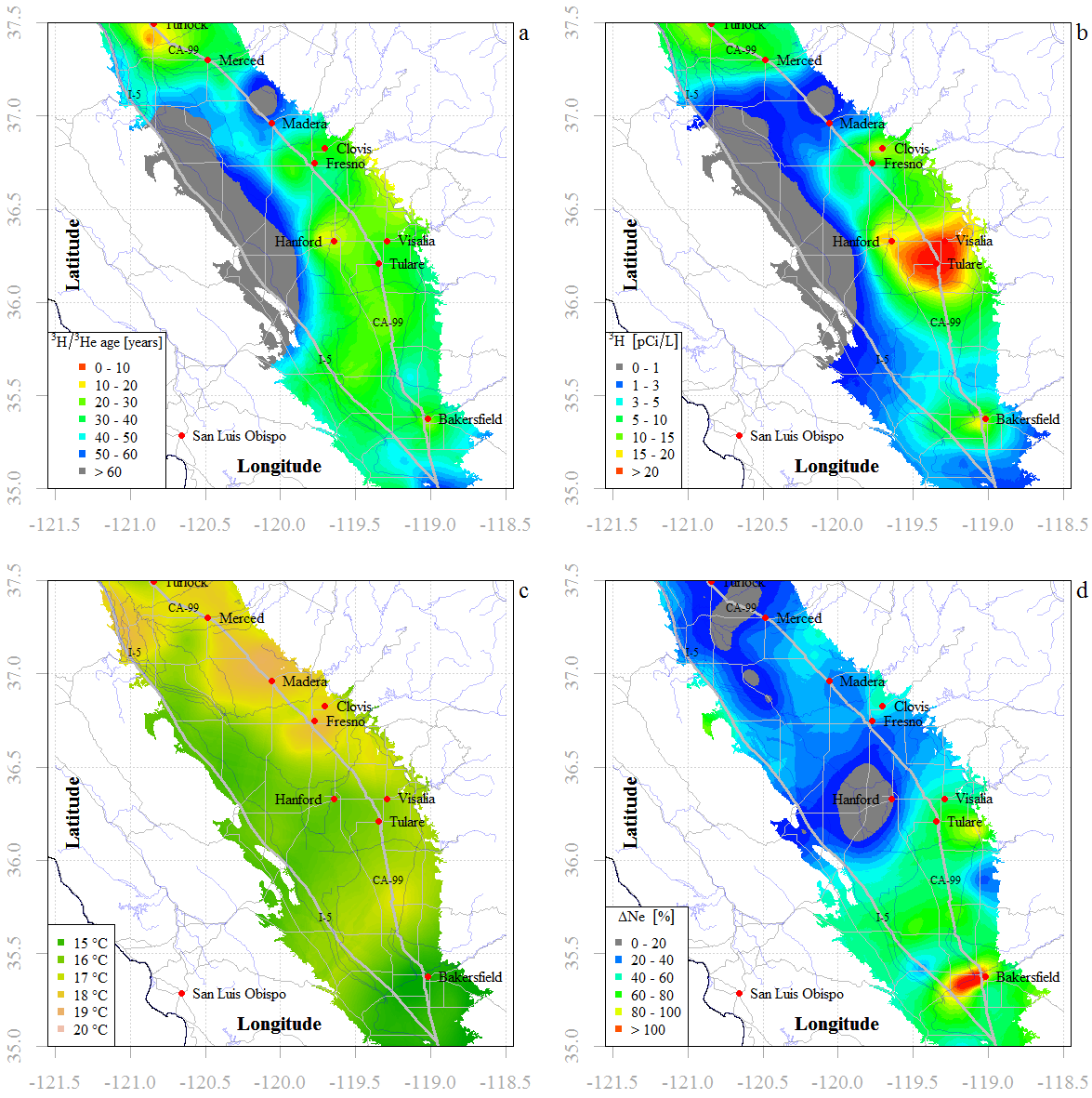

Figure 12: Predicted 3H/3He age (a), tritium concentration (b), noble gas recharge temperature (c) and excess air (d) in the San Joaquin Valley.

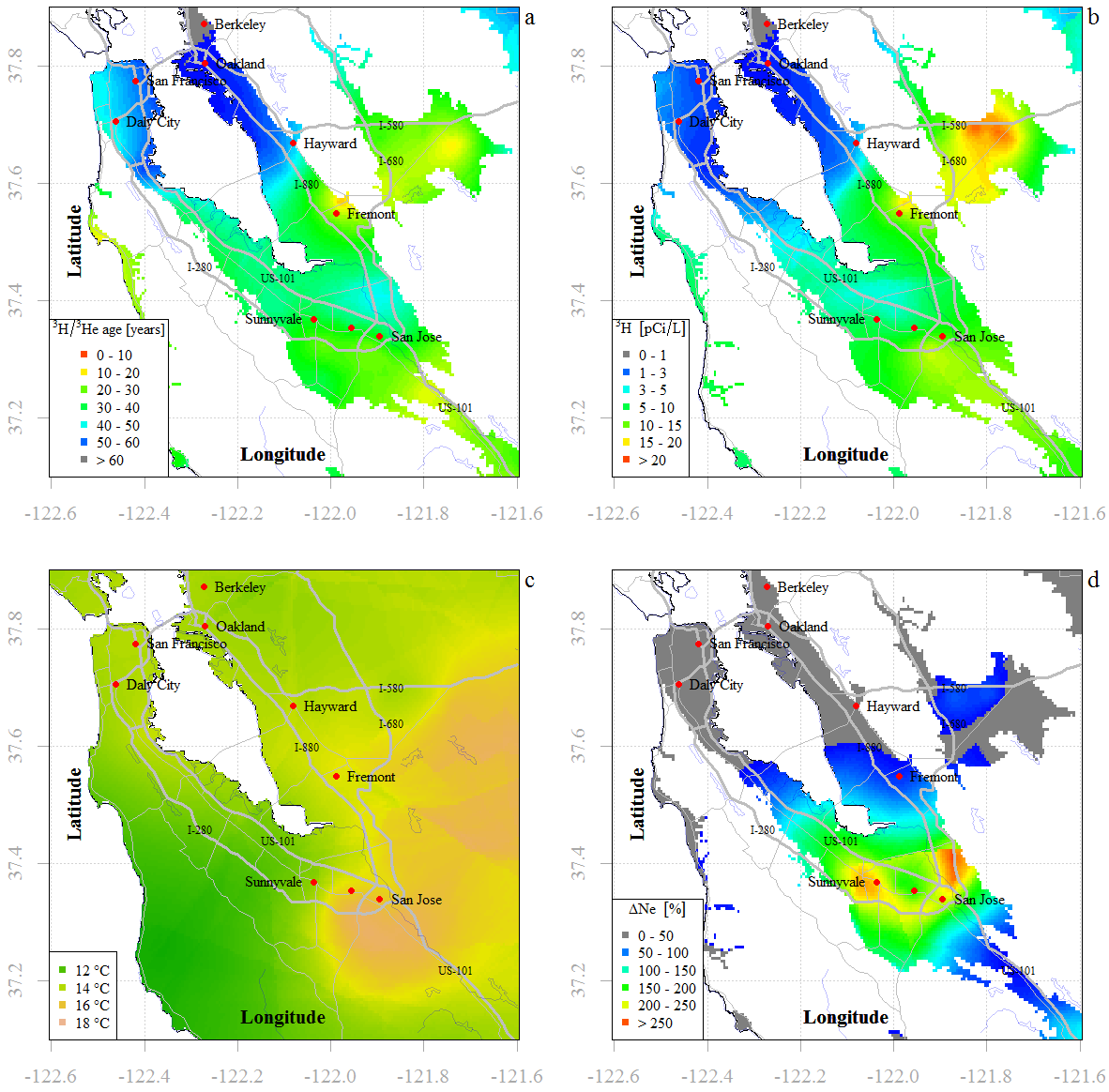

Figure 13: Predicted 3H/3He age (a), tritium concentration (b), noble gas recharge temperature (c) and excess air (d) in Santa Clara Valley.

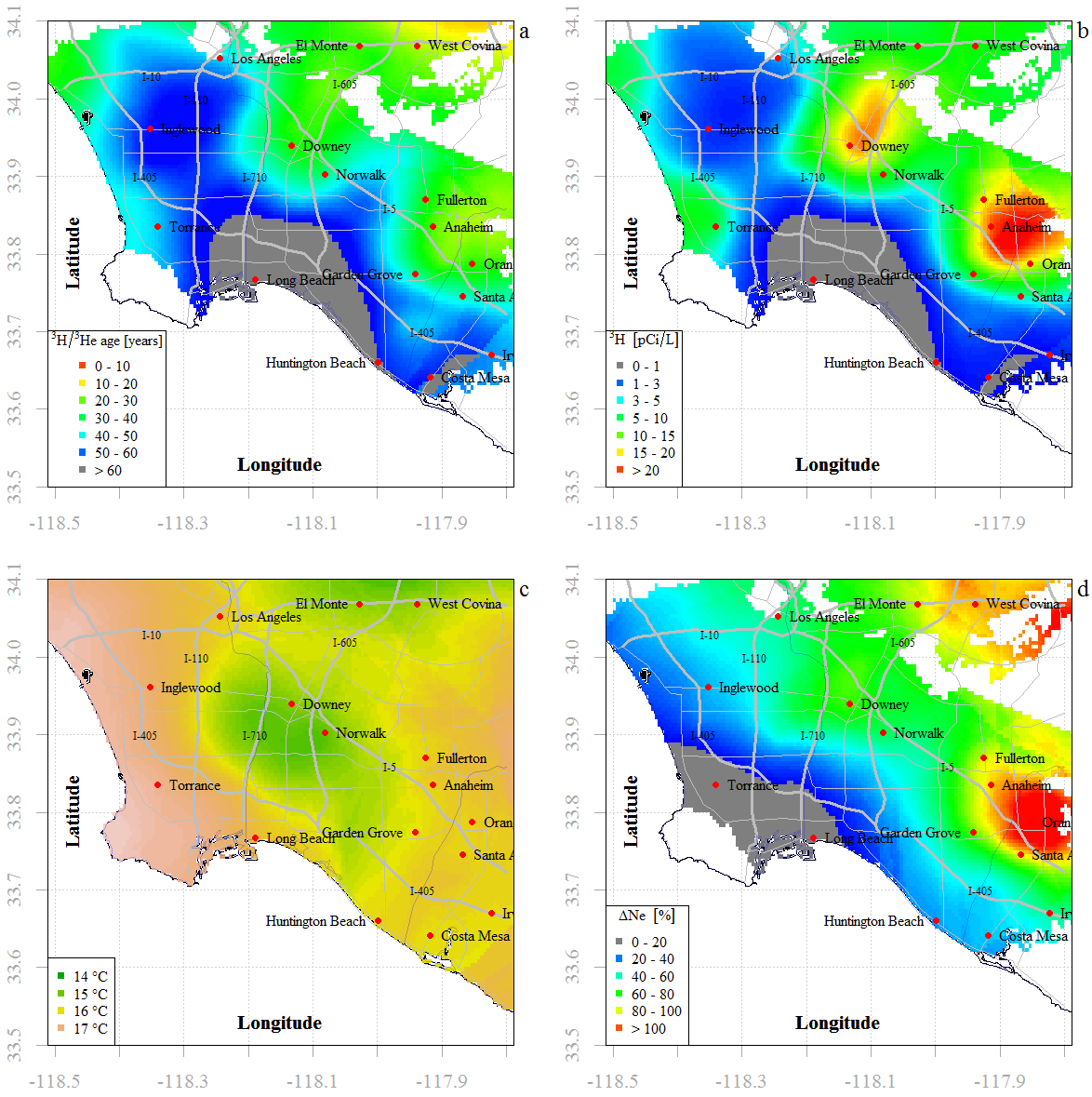

Figure 14: Predicted 3H/3He age (a), tritium concentration (b), noble gas recharge temperature (c) and excess air (d) in the Los Angeles Basin.

7 REFERENCES

GAMA Project reports are available on the State Water Board GAMA website: http://www.swrcb.ca.gov/water_issues/programs/gama/report_depot.shtml

Aeschbach-Hertig, W., F. Peeters, U. Beyerle, and R. Kipfer (2000), Palaeotemperature reconstruction from noble gases in ground water taking into account equilibration with entrapped air, Nature, 405(6790), 1040-1044.

Ballentine, C. J., and C. M. Hall (1999), Determining paleotemperature and other variables by using an error-weighted, nonlinear inversion of noble gas concentrations in water, Geochim Cosmochim Ac, 63(16), 2315-2336.

Belitz, K., N. M. Dubrovsky, K. Burow, B. Jurgens, and T. Johnson (2003), Framework for a Ground-Water Quality Monitoring and Assessment Program for California, Water Resources Investigation Report 03-4166Rep., USGS Water Resources Investigation Report 03-4166, Sacramento, CA, USA.

Belitz, K., B. Jurgens, M. K. Landon, M. S. Fram, and T. Johnson (2010), Estimation of aquifer scale proportion using equal area grids: Assessment of regional scale groundwater quality, Water Resour Res, 46(11), W11550, doi:10.1029/2010wr009321.

BerkeleyEarth.org (2013), ¼ Degree Gridded Average Temperature (TAVG) for Continental United States (CONUS) (http://berkeleyearth.lbl.gov/auto/Global/Gridded/), edited.

Bivand, R. S., E. J. Pebesma, and V. Gomez-Rubio (2013), Applied Spatial Data Analysis with R (Second Edition), Springer, New York.

Bolger, B. L., Y.-J. Park, A. J. A. Unger, and E. A. Sudicky (2011), Simulating the pre-development hydrologic conditions in the San Joaquin Valley, California, Journal of Hydrology, 411(3–4), 322-330, doi:http://dx.doi.org/10.1016/j.jhydrol.2011.10.013.

Bouwer, H. (2002), Artificial recharge of groundwater: hydrogeology and engineering, Hydrogeol J, 10(1), 121-142, doi:10.1007/s10040-001-0182-4.

Byrd, R. H., P. Lu, J. Nocedal, and C. Zhu (1995), A limited memory algorithm for bound constrained optimization, SIAM J. Sci. Comput., 16(5), 1190-1208, doi:10.1137/0916069.

California Department of Public Health (2014), DPH-14-003E Groundwater Replenishment Using Recycled Water.

Carle, S. F., B. K. Esser, and J. E. Moran (2006), High-resolution simulation of basin scale nitrate transport considering aquifer system heterogeneity, Geosphere, 2 (4, Special Issue: Modeling Flow and Transport in Physically and Chemically Heterogeneous Media), 195-209, doi:UCRL-JRNL-214721.

Cey, B. D., G. B. Hudson, J. E. Moran, and B. R. Scanlon (2008), Impact of Artificial Recharge on Dissolved Noble Gases in Groundwater in California, Environ. Sci. Technol., 42(4), 1017-1023.

Clark, J. F., G. B. Hudson, M. L. Davisson, G. Woodside, and R. Herndon (2004), Geochemical Imaging of Flow Near an Artificial Recharge Facility, Orange County, California, Ground Water, 42(2), 167-174, doi:10.1111/j.1745-6584.2004.tb02665.x.

Clarke, W. B., W. J. Jenkins, and Z. Top (1976), Determination of tritium by mass spectrometric measurement of ^{3}He, The International Journal of Applied Radiation and Isotopes, 27(9), 515-522, doi:http://dx.doi.org/10.1016/0020-708X(76)90082-X.

Deeds, D. A., J. T. Kulongoski, and K. Belitz (2012), Assessing California Groundwater Susceptibility Using Trace Concentrations of Halogenated Volatile Organic Compounds, Environmental Science & Technology, 46(24), 13128-13135, doi:10.1021/es303546b.

Department of Water Resources (2003), California's Groundwater - Bulletin 118, Updated 2003Rep.

Eaton, G. F., G. B. Hudson, and J. E. Moran (2003), Tritium-Helium-3 Age-Dating of Groundwater in the Livermore Valley of California, in Radioanalytical Methods in Interdisciplinary Research, edited, pp. 235-245, American Chemical Society, doi:doi:10.1021/bk-2004-0868.ch016.

Famiglietti, J. S., M. Lo, S. L. Ho, J. Bethune, K. J. Anderson, T. H. Syed, S. C. Swenson, C. R. de Linage, and M. Rodell (2011), Satellites measure recent rates of groundwater depletion in California's Central Valley, Geophys. Res. Lett., 38(3), L03403, doi:10.1029/2010gl046442.

Fram, M. S., and K. Belitz (2011a), Occurrence and concentrations of pharmaceutical compounds in groundwater used for public drinking-water supply in California, Science of the Total Environment, 409(18), 3409-3417, doi:http://dx.doi.org/10.1016/j.scitotenv.2011.05.053.

Fram, M. S., and K. Belitz (2011b), Probability of Detecting Perchlorate under Natural Conditions in Deep Groundwater in California and the Southwestern United States, Environ Sci Technol, 45(4), 1271-1277, doi:10.1021/es103103p.

Hanson, R. T., Z. Li, and C. C. Faunt (2004), Documentation of the Santa Clara Valley Regional Ground-Water/Surface-Water Flow Model, Santa Clara Valley, California. USGS Scientific Investigations Report 2004-5231. Sacramento, California 2004.

Heaton, T. H. E., and J. C. Vogel (1981), "Excess air" in groundwater, Journal of Hydrology, 50, 201-216.

Hudson, G. B., J. E. Moran, and F. Eaton Gail (2002), Interpretation of Tritium-^{3}Helium Groundwater Ages and Associated Dissolved Noble Gas Results from Public Water Supply Wells in the Los Angeles Physiographic BasinRep., 24 pp, Lawrence Livermore National Laboratory, UCRL-AR-151447.

Izbicki, J. A., C. L. Stamos, T. Nishikawa, and P. Martin (2004), Comparison of ground-water flow model particle-tracking results and isotopic data in the Mojave River ground-water basin, southern California, USA, Journal of Hydrology, 292(1-4), 30.

Jenden, P. D., I. R. Kaplan, R. J. Poreda, and H. Craig (1988), Origin of Nitrogen-Rich Natural Gases in the California Great Valley - Evidence from Helium, Carbon and Nitrogen Isotope Ratios, Geochim Cosmochim Ac, 52(4), 851-861.

Johnson, N. L., S. Kotz, and N. Balakrishnan (1995), Continuous Univariate Distributions, chapters 18 (volume 1) and 29 (volume 2), Wiley, New York.

Jurgens, B. C., M. S. Fram, K. Belitz, K. R. Burow, and M. K. Landon (2009), Effects of Groundwater Development on Uranium: Central Valley, California, USA, Ground Water, no-no, doi:10.1111/j.1745-6584.2009.00635.x.

Kendall, C., and T. B. Coplen (2001), Distribution of oxygen-18 and deuterium in river waters across the United States, Hydrol Process, 15(7), 1363-1393, doi:10.1002/hyp.217.

Kent, R., and M. K. Landon (2013), Trends in concentrations of nitrate and total dissolved solids in public supply wells of the Bunker Hill, Lytle, Rialto, and Colton groundwater subbasins, San Bernardino County, California: Influence of legacy land use, Science of the Total Environment, 452â€“453(0), 125-136, doi:http://dx.doi.org/10.1016/j.scitotenv.2013.02.042.

Landon, M. K., C. T. Green, K. Belitz, M. J. Singleton, and B. K. Esser (2011), Relations of hydrogeologic factors, groundwater reduction-oxidation conditions, and temporal and spatial distributions of nitrate, Central-Eastside San Joaquin Valley, California, USA, Hydrogeol J, 19(6), 1203-1224, doi:10.1007/s10040-011-0750-1.

Loosli, H. H. (1983), A dating method with ^{39}Ar, Earth and Planetary Science Letters, 63(1), 51-62.

Loosli, H. H., B. E. Lehmann, and W. Balderer (1989), Argon-39, argon-37 and krypton-85 isotopes in Stripa groundwaters, Geochim Cosmochim Ac, 53(8), 1825-1829.

Lundquist, J. D., M. D. Dettinger, and D. R. Cayan (2005), Snow-fed streamflow timing at different basin scales: Case study of the Tuolumne River above Hetch Hetchy, Yosemite, California, Water Resour Res, 41(7), W07005, doi:10.1029/2004wr003933.

Manning, A. H., D. K. Solomon, and S. A. Thiros (2005), H-3/He-3 age data in assessing the susceptibility of wells to contamination, Ground Water, 43(3), 353-367.

Massmann, G., and J. Sültenfuß (2008), Identification of processes affecting excess air formation during natural bank filtration and managed aquifer recharge, Journal of Hydrology, 359(3-4), 235.

McDermott, J. A., D. Avisar, T. A. Johnson, and J. F. Clark (2008), Groundwater Travel Times near Spreading Ponds: Inferences from Geochemical and Physical Approaches, Journal of Hydrologic Engineering, 13(11), 1021-1028.

McNab Jr, W. W., M. J. Singleton, J. E. Moran, and B. K. Esser (2010), California GAMA Special Study: Ion exchange and trace element surface complexation reactions associated with applied recharge of low-TDS water in the San Joaquin Valley, CaliforniaRep., 15 pp, Lawrence Livermore National Laboratory LLNL-TR-450392.

McNab, W. W., M. J. Singleton, J. E. Moran, and B. K. Esser (2007), Assessing the impact of animal waste lagoon seepage on the geochemistry of an underling shallow aquifer, Environmental Science and Technology, 41(3), 753-758.

Moran, J. E., H. Beller, G. F. Eaton, B. E. Ekwurzel, B. K. Esser, Q. Hu, G. B. Hudson, R. Leif, W. McNab, and C. Moody-Bartel (2005a), California GAMA program: Sources and transport of nitrate in groundwater in the Livermore Valley Basin, CaliforniaRep., 30 pp, Lawrence Livermore National Laboratory, UCRL-TR-217189.

Moran, J. E., S. F. Carle, and B. K. Esser (2010), California GAMA Special Study: Interpretation of Isotopic Data in the Sonoma Valley, CaliforniaRep., 31 pp, Lawrence Livermore National Laboratory LLNL-TR-427958.

Moran, J. E., B. K. Esser, D. Hillegonds, M. Holtz, S. K. Roberts, M. J. Singleton, and A. Visser (2011), California GAMA Special Study: Nitrate Fate and Transport in the Salinas ValleyRep., Lawrence Livermore National Laboratory, LLNL-TR-484186.

Moran, J. E., and M. S. Halliwell (2002), Characterizing Groundwater Recharge: A Comprehensive Isotopic Approach. American Water Works Association Research Foundation Report 90941, 199 pp.Rep.

Moran, J. E., and M. S. Halliwell (2003), Characterizing Groundwater Recharge: A Comprehensive Isotopic ApproachRep., 199 pp, American Water Works Association Research Foundation Report 90941.

Moran, J. E., G. B. Hudson, G. F. Eaton, and R. Leif (2002a), California Aquifer Susceptibility: A Contamination Vulnerability Assessment for the Santa Clara and San Mateo County Groundwater Basin: Lawrence Livermore National Laboratory (LLNL) Report, Contract No. W-7405-ENG-48, LLNL, Livermore, CA, 49 p.

Moran, J. E., G. B. Hudson, G. F. Eaton, and R. Leif (2004), California GAMA Program: A Contamination Vulnerability Assessment for the Bakersfield AreaRep. UCRL-TR-208179, 34 pp, Lawrence Livermore National Laboratory, UCRL-TR-208179.

Moran, J. E., G. B. Hudson, G. F. Eaton, and R. Leif (2005b), Results for the Sacramento Valley and Volcanic Provinces of Northern CaliforniaRep., 71 pp, Lawrence Livermore National Laboratory, UCRL-TR-209191.

Moran, J. E., G. B. Hudson, G. F. Eaton, and R. N. Leif (2002b), A Contamination Vulnerability Assessment for the Santa Clara and San Mateo County Groundwater BasinsRep., 49 pp, Lawrence Livermore National Laboratory, UCRL-TR-201929.

Moran, J. E., W. W. McNab, B. E. Esser, and G. B. Hudson (2005c), California GAMA program: Sources and transport of nitrate in shallow groundwater in the Llagas Basin of Santa Clara County, CaliforniaRep., 37 pp, Lawrence Livermore National Laboratory, UCRL-TR-213705.

Moran, J. E., M. J. Singleton, W. M. McNab, R. Leif, and B. K. Esser (2009), California GAMA Program: Tracking Water Quality Changes During Groundwater Banking at Two Sites in San Joaquin CountyRep. LLNL-TR-412861, 79 pp, Lawrence Livermore National Laboratory.

Natural Resources Conservation Service (2013), SNOTEL Data & Products, National Water And Climate Center (accessed 11/1/2013), edited.

Nir, A. (1964), On the interpretation of tritium "age" measurements of groundwater, Journal of Geophysical Research, 69(12), 2589.

Pebesma, E. J. (2004), Multivariable geostatistics in S: the gstat package, Computers & Geosciences, 30(7), 683-691, doi:http://dx.doi.org/10.1016/j.cageo.2004.03.012.

Poreda, R. J., T. E. Cerling, and D. K. Salomon (1988), Tritium and Helium-Isotopes as Hydrologic Tracers in a Shallow Unconfined Aquifer, Journal of Hydrology, 103(1-2), 1-9.

R Core Team (2013), R: A Language and Environment for Statistical Computing, R Foundation for Statistical Computing, Vienna, Austria.

Rademacher, L. K., J. F. Clark, G. B. Hudson, D. C. Erman, and N. A. Erman (2001), Chemical evolution of shallow groundwater as recorded by springs, Sagehen basin; Nevada County, California, Chem Geol, 179(1-4), 37-51.

Schlosser, P., M. Stute, H. Dorr, C. Sonntag, and K. O. Munnich (1988), Tritium/^{3}He Dating of Shallow Groundwater, Earth and Planetary Science Letters, 89(3-4), 353-362.

Schlosser, P., M. Stute, C. Sonntag, and K. O. Munnich (1989), Tritiogenic ^{3}He in Shallow Groundwater, Earth and Planetary Science Letters, 94(3-4), 245-256.

Shapiro, S. S., and R. S. Francia (1972), An approximate analysis of variance test for normality, Journal of the American Statistical Association, 67(337), 215-216.

Singleton, M. J., B. K. Esser, J. E. Moran, G. B. Hudson, W. W. Mcnab, and T. Harter (2007), Saturated zone denitrification: Potential for natural attenuation of nitrate contamination in shallow groundwater under dairy operations, Environmental Science and Technology, 41(3), 759-765.

Singleton, M. J., and J. E. Moran (2010), Dissolved noble gas and isotopic tracers reveal vulnerability of groundwater in a small, high-elevation catchment to predicted climate changes, Water Resour. Res., 46(10), W00F06, doi:10.1029/2009wr008718.

Singleton, M. J., J. E. Moran, B. K. Esser, S. K. Roberts, and D. J. Hillegonds (2010), California GAMA Special Study: An isotopic and dissolved gas investigation of nitrate source and transport to a public supply well in Califonia's Central ValleyRep., 32 pp, Lawrence Livermore National Laboratory LLNL-TR-427957.

Solomon, D., E. Cole, and J. Leising (2010), Excess air during aquifer storage and recovery in an arid basin (Las Vegas Valley, USA), Hydrogeol J, 1-8, doi:10.1007/s10040-010-0659-0.

Solomon, D. K., A. Hunt, and R. J. Poreda (1996), Source of radiogenic helium 4 in shallow aquifers: Implications for dating young groundwater, Water Resour. Res., 32(6), 1805-1813, doi:10.1029/96wr00600.

Solomon, D. K., S. L. Schiff, R. J. Poreda, and W. B. Clarke (1993), A Validation of the $^{3}H/^{3}He$ Method for Determining Groundwater Recharge, Water Resour Res, 29(9), 2951-2962.

Stute, M., M. Forster, H. Frischkorn, A. Serejo, J. F. Clark, P. Schlosser, W. S. Broecker, and G. Bonani (1995), Cooling of Tropical Brazil (5ºC) during the Last Glacial Maximum, Science, 269(5222), 379.

Stute, M., P. Schlosser, J. F. Clark, and W. S. Broecker (1992), Paleotemperatures in the Southwestern United States Derived From Noble Gases in Ground Water, Science, 256(5059), 1000-1003.

Surano, K. A., G. B. Hudson, R. A. Failor, J. M. Sims, R. C. Holland, S. C. MacLean, and J. C. Garrison (1992), Helium-3 mass spectrometry for low-level tritium analysis of environmental samples, Journal of Radioanalytical and Nuclear Chemistry, 161(2), 443-453, doi:10.1007/bf02040491.

Takaoka, N., and Y. Mizutani (1987), Tritiogenic ^{3}He in groundwater in Takaoka, Earth and Planetary Science Letters, 85(1-3), 74-78.

Thatcher, L. L., V. J. Janzer, and K. W. Edwards (1977), Methods for determination of radioactive substances in water and fluvial sediments. Techniques of Water-resources Investigations of the U. S. Geological Survey: Denver, CO; Book 5, Chapter A5; 79–81.

Visser, A., E. Fourré, F. Barbecot, L. Aquilina, T. Labasque, V. Vergnaud, and B. K. Esser (2014), Intercomparison of tritium and noble gases analyses, apparent $^{3}H/^{3}He$ ages and other derived parameters, Applied Geochemistry.

Visser, A., J. E. Moran, R. Aql, M. J. Singleton, and B. K. Esser (2013a), California GAMA Special Study: Examination of Water Quality in "Tritium-Dead" Drinking Water Wells. LLNL-TR- 558107. Lawrence Livermore National Laboratory. 54 p.Rep.

Visser, A., M. J. Singleton, D. J. Hillegonds, C. A. Velsko, J. E. Moran, and B. K. Esser (2012), California GAMA Special Study: Noble Gas Membrane Inlet Mass Spectrometry: A Rapid, Low-Cost Method to Determine Travel Times at Recharge Operations Using Noble Gas Tracers. Lawrence Livermore National Laboratory LLNL-TR-548931-Draft.

Visser, A., M. J. Singleton, D. J. Hillegonds, C. A. Velsko, J. E. Moran, and B. K. Esser (2013b), A membrane inlet mass spectrometry system for noble gases at natural abundances in gas and water samples, Rapid Communications in Mass Spectrometry, 27(21), 2472-2482, doi:10.1002/rcm.6704.

Vogel, J. C., L. Thilo, and M. Van Dijken (1974), Determination of groundwater recharge with tritium, Journal of Hydrology, 23(1-2), 131-140.

Werner, A. D., and C. T. Simmons (2009), Impact of Sea-Level Rise on Sea Water Intrusion in Coastal Aquifers, Ground Water, 47(2), 197-204, doi:10.1111/j.1745-6584.2008.00535.x.

Wilson, G. B., and G. W. McNeill (1997), Noble gas recharge temperatures and the excess air component, Applied Geochemistry, 12(6), 747-762.